A Computational Fluid Dynamics Analysis of an Offshore Multipurpose Platform Under Wave Effects

Auteur : Hernandez Escobar, Alejandra
Promoteur(s) : Rigo, Philippe
Faculté : Faculté des Sciences appliquées
Diplôme : Master : ingénieur civil mécanicien, à finalité spécialisée en "Advanced Ship Design"
Année académique : 2022-2023
URI/URL : http://hdl.handle.net/2268.2/18254

A COMPUTATIONAL FLUID DYNAMICS ANALYSIS OF AN OFFSHORE MULTIPURPOSE PLATFORM UNDER WAVE EFFECTS

ALEJANDRA HERNÁNDEZ ESCOBAR

ÉCOLE CENTRALE DE NANTES
SCHOOL OF ENGINEERING
OCEAN-MTECH-HOE-EMSHIP
NANTES
2023

A COMPUTATIONAL FLUID DYNAMICS ANALYSIS OF AN OFFSHORE MULTIPURPOSE PLATFORM UNDER WAVE EFFECTS

ALEJANDRA HERNÁNDEZ ESCOBAR

Master's thesis to qualify for Master's degree in Mechanics, specialized in Hydrodynamics for Ocean Engineering

Advisor(s)
Benjamin Bouscasse, Ph.D.

ÉCOLE CENTRALE DE NANTES
SCHOOL OF ENGINEERING
OCEAN-MTECH-HOE-EMSHIP
NANTES
2023

Approval note

First Reviewer
Name:
A liation:
Stree No.:
ZIP City:
Country:
Signature
Reviewer

Second Reviewer
Name:
A liation:
Stree No.:
ZIP City:
Country:
Signature

Nantes, August 21, 2023

DECLARATION OF AUTHORSHIP

August 21, 2023

Alejandra Hernandez Escobar \I declare that this thesis and the work presented in it are my own and have been generated by me as the result of my own original research. Where I have consulted the published work of others, this is always clearly attributed.Where I have quoted from the work of others, the source is always given. With the exception of such quotations, this thesis is entirely my own work. I have acknowledged all main sources of help.Where the thesis is based on work done by myself jointly with others, I have made clear exactly what was done by others and what I have contributed myself.This thesis contains no material that has been submitted previously, in whole or in part, for the award of any other academic degree or diploma. I cede copyright of the thesis in favour of the University of Centrale Nantes".

Date:
Signature:

Acknowledgements

The author would like to thank the members of the Research Laboratory in Hydrodynamics, Energetics, and Atmospheric Environment (LHEEA) at Ecole Centrale Nantes for their support in this project.

The development of this research was only possible thanks to the help of Benjamin Bouscasse, Ph.D., promoter of this thesis and coordinator of the Interfaces & Interactions in Numerical & Experimental Hydrodynamics (IIHNE) research group, and Lionel Gentaz, Ph.D., adviser and coordinator of the Mechanical Engineering master for EmShip+ students at ECN. I want to express my deep appreciation to them for enriching this project with scienti c knowledge, guidance, and encouragement.

Sincere thanks to Gaspard Engel, Ph.D., and Moran Charlou, Ph.D., who sel essly replied to my inquiries when having trouble with the numerical tool's implementation and understanding.

Finally, the author wishes to express immense gratitude towards family and friends for always being present, supporting, and believing in this project and the curious person behind it. I dedicate this thesis to you all.

Abstract

This project aims to bring a new perspective to the line of research in ocean engineering, particularly for the design and analysis of multipurpose platforms. This is to be achieved by analyzing some parameters on the Blue Growth Farm platform to contribute to the design and assessment process from a numerical point of view. This type of structure plays a fundamental role in the initiatives towards the e cient use of the marine environment for clean sources to supply the ever-increasing energy and food demand. Moreover, they try to combine di erent mechanisms and systems to ensure maximum utilization of the ocean's space and resources. The proposed research includes three work fronts: rst, the analysis of the platform's quasi-static behavior through the implementation of numerical simulations in transient states without the in uence of waves to evaluate how changes in the computational domain and spatial discretization a ect the results. Second, the proposal of a methodology for regular and irregular wave generation in a numerical wave tank when implementing wave-generation and absorption models. Third, the set-up and discussion around wave-structure interaction simulations considering the moored platform under the in uence of regular and irregular waves This is to be achieved by means of the nite volume method coupled with the in-house library FoamStar, which is based on OpenFOAM-5 and has similar capabilities to the InterFoam and Waves2Foam solvers. This work is framed within the Blue Growth Farm project within the framework of the European Union's Horizon 2020 research and innovation program. Thus, the present research aims to present the second attempt to validate the experimental results from the BGF project with the use of numerical simulations. The aim is that the guideline into the software environment and its particularities allows future researchers to evaluate and assess the design of o shore structures towards the nal goal of a successful recovery of energy and food to avoid or reduce undesirable e ects in the marine environment.

KEYWORDS:

Blue Growth Farm, Multipurpose Platform, Floating O shore Wind Turbine, Wave-Energy Coverter, Aquaculture, Computational Fluid Dynamics, FoamStar, OpenFOAM.

Contents

List of Figures

Pag.

List of Tables

GLOSSARY

BGF: Blue Growth Farm.

FOWT: Floating O shore Wind Turbine.

WEC: Wave-Energy Converter.

MPP: Multi-purpose platform.

RAO: Response Amplitude Operator.

PSD: Power Spectral Density.

OWC: Oscillating Water Column.

ORE: O shore Renewable Energy.

CFD: Computational Fluid Dynamics.

RANSE: Reynolds Averaged Navier-Stokes Equations.

RBM: Rigid Body Motions.

FVM: Finite Volume Method.

FSI: Fluid Structure Interaction.

WSI: Wave Structure Interaction

MRE: Marine Renewable Energy.

HIL: Hardware-In-the-Loop.

BC: Boundary Condition.

FFT: Fast Fourier Transform.

EU: European Union.

Part I

Introduction

Chapter 1

Introduction

1.1 MOTIVATION

Oceans have historically played a vital role in the construction and growth of human society. Archaeological traces of the first human aquatic exploitation have been found to date back to over 2 million years ago, and the active use of marine resources like shellfish, fish, and other marine animals seems to have happened much later, possibly started by Homo sapiens, known as modern humans (Ono, 2016). Marine environments were humans' last target for migration and colonization after being birthed in and around the inner forest environment over 600 million years before. However, as science and technology have displayed exponential growth over the past few hundred years, humans have been trying to study and exploit what the ocean - the largest ecosystem in the world - has to offer to an increasing human population. In this effort, humans have realized the multiple sources of energy present in the marine environment, such as wind, waves, tides, currents, temperature, and pressure gradients (Abhinav et al., 2020). Then, it has been the labor of modern engineers and scientists to study how that energy can be safely and sustainably retrieved, at the same time as learning every time more about the complex and intricate physical phenomena that open sea states poses.

Fortunately, this labor has paid off, since as noted by the European Commission, (European comission and Fisheries, 2012), by the year 2012, 75% of Europe's external trade, and 37% of the trade within the EU was seaborne, representing at the time 5.4 million jobs and a gross added value of just under €500 billion per year. Furthermore, beyond economic reasons, today's globalized and rapid-changing world has brought new challenges and insights, forcing humanity to expand the horizons of what is known and explored. Modern society is experiencing an increasing awareness regarding the finite nature of land and freshwater resources and the need to reduce anthropogenic greenhouse gas emissions, which have been identified as the principal cause of climate change (European comission and Fisheries, 2012). In addition to encouraging the building of offshore renewable energy facilities, the goal of reducing greenhouse gas emissions has also increased the need for energy conservation and given people more justifications to choose seaborne transportation over land and air transportation because of the lower emissions per tonne-kilometer.

All these factors have given rise to recent efforts focusing on taking advantage of the opportunity offered by offshore renewable energy resources, aiming for technological progress that allows working offshore in ever-deeper waters and solving the problem of how the 71% of the planet that is ocean can deliver human necessities such as food and energy in a way that is more sustainable and conscious. Furthermore, the ever-increasing constraints limiting the possibilities for the expansion of inland and near-shore fisheries have boosted offshore aquaculture as a viable alternative for increasing global seafood production; this is an essential consideration because the Food and Agriculture Organization (FAO) anticipates that by 2030, demand for seafood would exceed supply by 40 million metric tonnes (FAO, 2006). In this regard, as mentioned in (Abhinav et al., 2020), offshore farming offers several advantages - increased possibilities for expansion, reduced exposure to pollution from human sources, and the potential of co-locating infrastructure with Offshore Renewable Energy (ORE) systems to reduce competition for space.

The successful commercialization of maritime energy and food sources is crucial in providing secure, sustainable, and economical energy and food. And currently, the potential for the marine environment is still far from being realized and used. Offshore wind projects, in conjunction with onshore wind facilities, may produce 2600 TWh of energy at a competitive price, accounting for up to 20% of total electricity demand in Europe (Ruzzo et al., 2021). Soon, the oceans will be subjected to massive development of marine infrastructures, including offshore wind, tidal, and wave energy farms and constructions for marine aquaculture (Zanuttigh et al., 2015). Wind turbines, offshore terminals, pipelines, motorways at sea, and fish farms will occupy more and more marine space in the future; this poses new challenges since the development of these facilities will unavoidably exert environmental pressures on marine ecosystems.

There is, therefore, an urgent need to increase awareness among private and public bodies and to provide policymakers with knowledge and tools to optimize the design and the location of these activities, thus preserving the marine ecosystem and ensuring that the economic costs, the space management and the environmental impacts of these activities remain within acceptable limits while aiming to keep up with the ever-increasing global food and energy demand, which is forecasted to rise 50% by 2030 (Zanuttigh et al., 2015). As a result, there is now an opportunity for blue growth - the long-term European strategy to harness the untapped potential of Europe's oceans, seas, and coasts. \Blue Growth"and \Blue Economy"are de ned by the World Bank as: \the sustainable use of ocean resources for economic growth, improved livelihoods and jobs, while preserving the health of ocean ecosystem"(Abhinav et al., 2020).

1.2 PROBLEM STATEMENT

O shore aquaculture and renewable energy production are promising candidate solutions, especially in a combined hosting structure. In particular, multi-purpose arrangements combining renewable energy from the sea, aquaculture, and transportation facilities can be considered a challenging yet advantageous way to boost blue growth (Zanuttigh et al., 2015). A Multi-Purpose Platform (MPP) is an o shore system designed to serve the purposes of more than one o shore industry. They are emerging as a promising concept in ocean engineering applications, thanks to their capability of cost reduction, infrastructure sharing, modularization, and system integration, which allows using the locally produced energy to feed the platform's di erent functionalities (Ruzzo et al., 2021).

While several platforms have been previously proposed and investigated, there is a push to raise the Technology Readiness Level (TRL) of such concepts by testing the proposed multi-purpose system in a relevant environment (Ruzzo et al., 2020). \The Blue Growth Farm"(BGF) has arisen in this context. It is an ongoing H2020 European project aimed at the development, engineering, and demonstration of a new oating multi-purpose platform concept - an MPP consisting of a large wind turbine and a series of Wave Energy Converters (WECs) supported by a platform with an internal pool used as aquaculture sh cages (Li et al., 2020). The proposed platform considers a DTU 10 MW o shore wind turbine, a reference model for studies combining on-site electric energy from wind and Oscillating Water Column (OWC) WECs. Furthermore, the proposed WECs were inspired by the REWEC3 patented concept (Boccotti, 2002), and considered in the overall conception as embedded in the frontal breakwater. Finally, the sh cages take advantage of the protected internal pool and the wave energy absorbed by the WECs. They share the oater and the mooring system with the platform while providing additional damping to the oating platform (Ruzzo et al., 2020).

When dealing with an innovative MPP concept, i.e., the oating platform of the present study, it is crucial to take into account multiple issues, including the proper dynamic coupling of the di erent sub-systems, potential hydro-elastic e ects due to the relatively large size of the platform (Li et al., 2020), scaling laws discrepancies between the sub-systems, and the need for considering large physical models to achieve a reliable similitude between the full-scale structure and its physical model counterpart (Ruzzo et al., 2021). Therefore, regarding the signi cant complexity of the coupled dynamic behavior of the proposed concept, model tests are essential to investigate the most relevant physical phenomena. Two experimental campaigns took place in this context. The rst one was concluded in October 2019 at the \Hydrodynamics and Ocean Engineering Tank"at Ecole Centrale de Nantes (France) by a 1:40 scaled con guration (Jeremy et al., 2022), and several experimental data about the overall platform dynamics have been collected, as never achieved in the past, (Li et al., 2020).

The framework developed to support those experimental results is presented in this study, with a focus on numerical simulations aimed at validating the appropriateness and correctness of the experimental campaign, as well as taking an additional step towards a better understanding of the complex dynamics of these novel o shore structures and supporting their design.

1.3 OBJECTIVES

The purpose of this research project is to evaluate a realistic model of an o shore multipurpose platform under various wave situations. The goal is to describe the numerical activities, ne-tune the mechanisms and strategies for modeling the physical test environments, and establish an accuracy threshold between the experimental and numerical results, with the ultimate goal of making a practical contribution to the state-of-the-art research on MPP concepts.

1.3.1 GENERAL

Analyze the response to hydrodynamic forces acting on a realistic o shore platform designed for the European Blue Growth Project using the Finite Volume Method (FVM) in the open-source software foamStar, as well as a brief state-of-the-art focused on relevant numerical and experimental approaches attempting to reproduce and understand the response of multipurpose o shore structures to wave forces. The goal is to provide some information for future academics entrusted with analyzing MMP designs in the context of numerical simulations.

1.3.2 SPECIFIC

- Present a brief state of the art on numerical and experimental campaigns addressing the study of hydrodynamics for ocean engineering for combined O shore Renewable Energy systems (ORE): Multipurpose or Large Floating O shore Platforms (MMP/LFOP).
- Describe numerical considerations and methodology used to replicate some of the experimental ndings from the Blue Growth project.
- Analyze the in uence of two wave- eld scenarios on the BGF's motions, loads, wave elevation, and mooring tension forces through three-dimensional quasi-static and dynamic approaches.

1.4 CONTEXT

This project was developed at the Research Laboratory in Hydrodynamics, Energetics and Atmospheric Environment (LHEEA), based in Ecole Centrale Nantes, Fr. The laboratory is a CNRS mixed research unit tasked with both advancing theoretical knowledge and resolving concrete problems around four scienti c themes: free-surface hydrodynamics, uid-structure interactions, dynamics of the atmosphere and systems approach for ground and marine propulsion systems. (LHEEA, 2023)

More speci cally, the research falls under the Interfaces & Interactions in Numerical and Experimental Hydrodynamics (IIHNE) research group, which studies complex hydrodynamic interactions between free-surface ows and solid bodies. The research group combines advanced experimental and numerical methods in marine hydrodynamics. First, the Ocean Engineering basin team aims to design, manufacture, and implement the experimental models tested in the basins, as well as operate, maintain, and upgrade the testing facilities that include a 140m-long by 5m-wide and 3m-deep Towing tank, a 50m-long by 30m-wide and 5m-deep Hydrodynamic and Ocean Engineering tank, a 20m-long by 9.5m-wide and 1m-deep Shallow water tank, and a 10m-long, 2m-wide and 1.10m-deep Recirculating canal. Second, regarding the numerical e orts, the laboratory bene ts from Bureau Veritas' establishment as Centrale Nantes Chair in hydrodynamics and marine structures (2016-2025) for the development of innovative numerical methods in hydrodynamics, including the development of in-house software foamStar, among others.

This project constitutes a second attempt to validate numerical simulations' results when compared against the experimental ones obtained in the campaign described in (Ohana et al.,

2023) and (Ruzzo et al., 2020). The numerical modeling of the BGF platform was attempted on foamStar, initially setting up the test case for regular and irregular waves using the stream function theory. This initial simplified setup rendered results without them being consistent in comparison with the experimental data. It is worth mentioning that it was a brief and pressed attempt, the reason why the author was subsequently charged only with following up with the research as part of the master's thesis to qualify for a Master's degree in Mechanics, specializing in Hydrodynamics for Ocean Engineering.

It is relevant to mention, as a final remark regarding the context of the present research, that during the development of this study (which started in March 2023), the available computational resources at the LHEEA lab were under compromise since the Centrale Nantes' supercomputing cluster "Liger" was closed down from the beginning of May 2023, due to Centrale Nantes's adhesion to the Groupement Ligérien en Calcul Intensif Distribué (GLiCID). The last one encompasses brand new computing facilities with higher performance, hosted at the Ecole Centrale de Nantes, but is also the mesocentre of the Pays de la Loire region (GLiCID, 2023). In this sense, and considering that the GLiCID cluster started to be functional from the first of August 2023, most of the numerical simulations and analyses presented in this thesis were not performed on a supercomputing cluster but combining two desktop computers, resulting in a total of eight cores available for parallel computations (four at each desktop). Of course, this represented a challenge for the flow of the study and its completion in due time since the cases to simulate inherently require significant resources.

1.5 THESIS OUTLINE

This thesis brings concepts from hydrodynamics to ocean engineering and the use of in-house code, FoamStar, for CFD simulations. With these tools in hand, the study proposes a means to analyze the quasi-static and dynamic behavior of an offshore structure when subjected to different environmental conditions and to describe the methodology and mathematical criteria employed to reproduce the results subjected to analysis. The study means to give some insight – a first approximation if you would like – to understand how the finite volume approximations of different wave models intervene in obtaining accurate results when comparing them to the experimental approach. The theme is in nature for someone who feels fine reading the language that is math, besides having a background in continuum mechanics, OpenFOAM environment, and programming. Acknowledging that, in general, it is not very common to find someone who feels comfortable around all the abovementioned topics, this thesis attempts to cover the tools for understanding the whole matter. Because of this and since the study covers various aspects, the text is rather long; consequently, the author appeals to the reader's patience. The description of the thesis organization herein looks forward to informing the reader about where and what to find to allow each person to adjust the reading to their interests.

The booklet has three parts that follow this introductory one: (II) theoretical and numerical modeling; (III) naval application; and (IV) an epilogue. The first chapter briefly delineates the background for the present reasearch in terms of the state of the art for the topics of interest. The second part includes Chapter 2 and 3. Chapter 2 deals with the theoretical and mathematical aspects of the study and focuses on introducing the equations that allow us to model the phenomena of interest. Chapter 3, Numerical Methods, briefly describes the method for discretizing the equations and introduces the reader to the OpenFOAM software, the foamStar development, and the solver algorithm used for the computations.

Two chapters integrate Part III. In Chapter 4, Blue Growth Farm, the author describes the case architecture (case set-up) in foamStar used for the computational simulations containing the BGF geometry. The description includes pre-processing techniques, boundary conditions, schemes, and all relevant information so that it may be easier for a third party to try and reproduce. Furthermore, Chapter 5, Results and Discussion, wrap up one of the purposes of the thesis: analyzing the obtained results, the influence that a change in wave model can have on them, and their correspondence with the experimental data.

Part IV brings commonplace conclusions and further work. The thesis concludes with Appendix A, which depicts illustrations of the foamStar case architecture and commands used for the CFD simulations. At the very end, the author provides the pertinent references that were used to guide and enhance the research.

Chapter 2

Background

This chapter reviews experimental and numerical methodologies used by other researchers to tackle the coupled-dynamic analysis of ORE systems, emphasizing MPPs, WECs, and aquaculture cages. This section does not seek to o er a comprehensive review, but rather to illustrate and discuss the context in which the current study is undertaken. Although it's conceivable that some—or many— pertinent studies weren't cited in the text, the following is intended to provide the reader with a quick overview of the references that were deemed critical for the construction of this thesis.

2.1 MULTIPURPOSE PLATFORMS

Previous research initiatives have investigated technologically advanced and sustainable solutions for the Blue Growth Economy. In this sense, the idea of o shore multi-purpose (MP) structures has drawn attention from the scienti c community because of their potential to take advantage of synergies between ORE and aquaculture systems while averting potential con icts in their close co-location, in addition to the opportunity for marine space optimization through shared infrastructure. The European Commission has made considerable e orts in this regard, and they paved the way for the Blue Growth concept.

From 2007 the EU's Seventh Framework Programme (FP7) focused on the o shore renewable sector and funded two worth-mentioning research projects. First, the **ORECCA** project (O shore Renewable Energy Conversion platforms-Coordination Action) aimed to create a framework for knowledge sharing and to develop a road-map for research activities in the context of o shore renewable energy (Sedgwick,). In particular, the project aimed to stimulate collaboration in research activities among European research organizations, industry stakeholders, and policymakers to try and overcome barriers to the development of the sector and stimulate these communities to take the necessary steps to foster the development of the o shore renewable energy sector in an environmentally sustainable way. The results included recommendations to the EU and member state administrators divided into four categories: Finance; technology; infrastructure; and \Environment, Regulation & Legislation".

Second, the **MARINA** project attempted to provide a set of protocols covering the engineering and economic evaluation of MP Marine Renewable Energy (MRE) platforms, taking into account also non-energy uses, planning & consenting issues surrounding their deployment (Auer,). One of their work packages called \WP7: Critical Component Engineering" managed to identify the critical components for wind-and-wave-energy integrated platforms, develop risk assessment methodologies, and produce a toolbox to support the design and evaluation of system components. The fourth work package \WP4: Synthesis modeling and testing" was led by the Norwegian University of Science and Technology (NTNU) and involved considerable e orts in the instrumentation of test models —some of them conducted at ECN!— to measure motions between multiple bodies, their contact force, internal structural loads, free surface elevation, pressure in the air chambers, and mooring line tensions. Moreover, the model testing led to the development of experimental techniques and provided a basis for validating numerical methods and tools. The researchers used the numerical tool Simo-Ri ex-AeroDyn and focused on simpli ed approaches to obtain global responses under both wind and wave loads. The comparison of the regular and irregular wave cases showed that the motion responses predicted by the numerical tools (such as Simo-Ri ex-AeroDyn, including rst and second-order wave loads and coupled with wind turbine aerodynamics) compared favorably with the model test results as long as there were no strongly nonlinear hydrodynamic loads. They concluded that strongly nonlinear wave loads, such as slamming loads, could not be modeled with simpli ed methods.

Because of what these experiments revealed, the European Commission funded three sibling research studies between 2012 and 2021: H2Ocean, MERMAID, and TROPOS, through the PF7 program (Perez, 2014). The **H2Ocean** initiative (Comission, 2017) was active for two years, from 2012 to 2014. It was part of the \Ocean of Tomorrow" joint call to create a proof-of-concept novel design that allowed the integration of ocean renewable energy with aquaculture, o shore transit facilities, environmental monitoring, and other relevant activities. The conversion of o shore energy into hydrogen is a unique feature of the H2OCEAN concept. The produced hydrogen could be stored and used for re-fueling at the platform or shipped to shore. For this purpose, the project made several novel developments, including: integrating into the WEC a vertical axis wind turbine (VAWT) and modeling the coupling e ects, high-pressure membranes for the reverse osmosis units in charge of producing water, a fully integrated multi-trophic aquaculture system, a novel type of oating digester to mitigate organic pollution caused by the system, and a web-based geographic information tool incorporating data for selected locations in uencing the establishment and operation of an H2Ocean platform.

The **MERMAID** consortium consisted of 29 European partners in charge of developing o -shore platforms concepts for the multi-use of ocean space (energy extraction, aquaculture, and platform-related transport) (Pirlet, 2014). The project did not intend to create new platforms but to test various concepts combining existing with new structures and evaluating their response on representative sites to account for di erent environmental characteristics. The aim was to determine the best practices and most e ective ways for installing, maintaining, and operating a multi-purpose o shore platform considering the economic and environmental bene ts and long-term consequences. Four o shore test study sites were selected to represent di erent environmental, social, and economic conditions: The Baltic Sea, a typical estuarine area with fresh water from rivers and saltwater; the trans-boundary portion of the North Sea-Wadden Sea, an active morphology site; the Atlantic Ocean, a typical deep water site; and the Mediterranean Sea, a sheltered deep water site. They concluded that integrating various user functions in a multi-use o shore platform provides signi cant bene ts regarding the shared use of infrastructure, resources, and services. Furthermore, they found that the combination of activities generally results in a reduced environmental impact compared to several single-use platforms and acknowledged the need for further optimization of integrated designs.

The full title of the **TROPOS** project is \Modular Multi-use Deep Water O shore Platform Harnessing and Servicing Mediterranean, Subtropical and Tropical Marine and Maritime Resources"(Brito, 2015). TROPOS had a total project duration of 3 years (January 2012-January 2015) and aimed at developing a oating modular multi-use platform system for use in deep waters, with an initial focus on Mediterranean and sub-tropical regions (Papandroulakis et al., 2017). The main objectives of the TROPOS project involved: the determination of the optimal locations for multi-use o shore platforms; the development of three novel, cost-e cient, and modular multi-use platform designs (at least one for each of the Mediterranean, subtropical, and tropical latitudes); and the assessment of the logistical requirements, economic viability, and environmental impact. Considering all the di erent aspects examined in the project, the Sustainable Service Hub on the Dogger Bank (North Sea, UK) turned out to be the most economically viable and ecologically sustainable concept. When focusing on transport and energy-related needs of the o shore renewable energy sector, the Sustainable Service Hub would signi cantly reduce the impact of o shore wind farms on ecosystems as most of the tra c would occur in a limited area within the wind farm site.

On the ground of these initiatives, MPPs are evermore emerging as viable solutions for a growing global population's coastal space, food, and energy demands in a world with nite resources. Furthermore, to this day, various studies on the combined use of multiple ocean resources have been conducted and reported by previous researchers. Luckily for the author, the research conducted in (Abhinav et al., 2020) provides a multidisciplinary state-of-the-art evaluation of multi-purpose platforms, including synoptic tables and a comprehensive snapshot that categorizes their references by industry (o shore renewables, aquaculture, both) and aspect (technological, environmental, socioeconomic). The article discusses several relevant projects funded to expand the knowledge and understanding of the combined use of multiple ocean resources. Moreover, concerning the numerical methods interest in this thesis— they presented a table summarizing the numerical modeling approaches used in previous studies for representing the aerodynamic aspects, ranging from a simple static wind drag force to the more accurate blade element momentum (BEM) theory. The authors also discovered that all the models used a wave di raction-based potential ow technique for the hydrodynamics investigation, and to model structural dynamics, rigid body or multibody techniques were used. They emphasized that o shore renewable energy (ORE) and aquaculture systems are the most attractive candidates for integration inside MPPs, although most of the literature focuses solely on coupled ORE applications. Some worthy e orts are addressed next in this regard.

Through their application to a case study in the Mediterranean Sea, (Zanuttigh et al., 2015) exploited and incorporated some of the MERMAID project's ndings. The project investigated the combination of aquaculture, energy generation, and energy storage or transfer. They ranked the potential solutions based on expert assessment and o ered a preliminary layout of the preferred multi-purpose installation for the case study. A key result was that wave energy arrays acted as a safeguard for aquaculture cages and should be installed on their exposed side and surrounding them in the direction of the more energetic wave states. To enhance wave energy generation and aquaculture protection in a bi-directional wave environment, the primary axis of the MPP should be almost perpendicular to the two prevailing directions of incoming waves.

Later, in 2020, (Li et al., 2021) suggested and examined the technological viability of an MPP idea within the context of the BGF project. The evaluation comprised a three-level approach for analyzing and supporting the complex dynamics of MPP structures. The rst level employed a 2D strip theory-based parametric analysis. Based on this analysis, the cross-section of the MPP support structure was optimized to ensure that the natural periods of the system were outside of the typical 1st-order wave force period range. The second level determined whether it was necessary or not to include the elasticity of the platform in the coupled model of dynamics; they used a 3D hydro-elastic nite-element model for modal analyses. It con rmed the feasibility of the rigid-body hypothesis for the dynamic study of the support structure and revealed that the vibration modes of the same were not excited by external loads. Finally, based on the results of the rst two steps, the third level included frequency and time-domain analyses regarding the platform as a rigid body. In the frequency domain, the researchers compared the predictions of two potential theory solvers (Ansys AQWA and Wadam) in a code-to-code validation approach. In the time domain, the authors created an aero-hydro-servo-elastic coupled model in SIMO/RIFLEX, and it was employed to get the structure's coupled dynamic response and ultimate limit state under joint wind-wave excitations. The study investigated motion and structural responses in several operational and survival states. The numerical model had several simpli cations and limitations, particularly concerning the WEC representation as a linear damping force; nonetheless, it provided a framework for the primary assessment of structural dynamic characteristics and feasibility. Furthermore, the research con rmed the technical feasibility of the BGF MPP design.

Beyond the numerical models and due to the signi cant complexity of the coupled dynamic behavior of the BGF MPP, model tests are essential to understand the physical phenomena and calibrate the numerical models. In this regard, additional issues emerge since the sub-systems integrated into the structure often follow various scaling laws and may require considerable physical models to obtain excellent agreement between the full-scale and their physical model counterparts. The article by (Ruzzo et al., 2021) reviews some fundamentals of the scaling theory and extensively discusses its application to speci c cases of interest. In particular, scaling strategies for oating hulls, mooring systems, wind turbines, oscillating water column (OWC) wave energy converters (WECs), and net cages for aquaculture were considered individually. The study provides a critical and pertinent analysis of the relevance of the scaling factor and strategy, which the author encourages to read to those interested in the experimental hydrodynamics details, as the cases evaluated represent the most frequent sub-systems proposed for MPPs and the study also presented possible elements of integration between the sub-systems.

To conclude this section, the paper presented by (Ruzzo et al., 2020) represents the framework and reference for the present thesis. It describes the arrangement of the experimental activities for the Blue Growth project, focusing on the appropriateness of the up-scaling methodology and test environments. The authors employed Froude scaling principles to design the models and presented results from two experimental activities. The rst campaign concluded in October 2019 at the \Hydrodynamics and Ocean Engineering Tank"at Ecole Centrale Nantes (ECN) using a 1:40 steel scaled structure. The campaign conducted 229 tests in total, including pull-out and free decay tests in the absence of wind and waves, and regular and irregular wave scenarios for various wave directions (0, 22.5°, 45°), with and without wind. The study accounted for turbulent wind conditions using a hybrid Hardware-In-the-Loop (HIL) technique. Data from a video motion capture system was combined with inertial motion unit measurements through a Kalman lter when measuring the wind turbine tower's bending motion. The WECs' design did not fully exploit the Froude scale similarity, but pressure transducers and resistive probes allowed them to measure the air chamber pressures, the water column displacements, and the exciting wave pressure at the water column inlet. Considering that the main forces transmitted to the oater by the sh nets are hydrodynamic ones, the authors used a screen model that assumes the shnet as a set of panels, and hydrodynamic coe cients would depend on solidity ratio (S) and the Reynolds number (Re). In this way, the sh nets' S was constant and the same as the full-scale one. The study included di erent test scenarios: the MPP alone, without sh nets and active WECs, with active WECs only, and with both.

The second experimental activity was to planned to be at sea, at the Natural Ocean Engineering Laboratory (NOEL) of Reggio Calabria, by a 1:15 scaled con guration. The experiment aimed to obtain a more detailed representation of the structure and its behavior by accounting for the interaction between sub-system components in an outdoor marine environment. The framework suggested in the paper can be helpful for subsequent experimental campaigns on related ideas, and it is unquestionably the foundation for the numerical validation attempt made in the current study.

Part II

Theoretical and numerical modeling

Chapter 3

Mathematical models

As expressed by Marcus du Sautoy, \The power of mathematics lies in its ability to generalize results beyond their original context and to nd applications far beyond anything anyone may have expected."In this chapter, the author provides a general description of the mathematical models and tools that are essential in the context of incompressible two-phase ow. The aim is to present a discussion on the governing equations, the physics they attempt to represent, and the assumptions made for the sake of engineering.

3.1 FLUID-STRUCTURE INTERACTIONS AND FIELD'S DESCRIPTION

O shore platforms operate under various environmental conditions, such as waves, winds, and currents. From the engineering point of view, these conditions represent external forces that will interact with the platform as long as it remains in service. When studying the design or optimization of any o shore platform, rst, it is imperative to understand that the problem involves the dynamic behavior of a structure, considered exible, when in the presence of uids (water, air).

The computation of Wave-Structure Interaction (WSI) problems requires the solution of the underlying governing equations for the uid mechanics, the structural (or solid) mechanics, and the coupling equations between them. As each of the two sub-problems constitutes, on its own, a considerable challenge, it is no surprise that developments in the numerical modeling and results for the coupled problems under di erent contexts are rarely spread (Richter, 2017). Depending on the application, the researchers could nd diverse demands for the mathematical description, assumptions, and coupling strategies when attempting numerical modeling. Research under the context of o shore platforms is usually interested in studying several variables: from the ow eld, changes in free-surface elevation, high pressure and velocity areas, turbulence e ects, and possible breaking or sloshing e ects. From the structural mechanics, principal stresses or strains on the structure, and wind-turbine-tower bending moments, especially at the base. From the coupling between models, the platform's global body motions, accelerations, and forces at the mooring lines.

But before jumping into equations, it is essential to bring the kinematics discussion to the table since kinematics is the part of continuum mechanics that describes the motion and allows building the di erential equations, which intend to replicate the fundamental principles of physics through mathematical relations. Kinematics can be described under two approaches when solving the elds of interest: the Eulerian or Lagrangian frames. Understanding their de nition and di erences constitutes what the author believes to be the starting point when attempting to tackle any Fluid-Structure Interaction (FSI) problem, in this case, WSI.

The Eulerian frame, where kinematics description happens in a \current"con guration, is often used by researchers to analyze uid ows. In other words, the continuum moves with respect to the grid while the domain remains xed. Under such considerations, one can solve and handle signi cant distortions in the continuum motion, but generally at the expense of precise interface de nition and the resolution of ow details,(Donea et al., 2004). Moreover, as explained by (Richter, 2017), moving domains are typical in structure mechanics since the movement of the solid is precisely the unknown solution. Therefore, it is common practice to simulate the motion of solids using the Lagrangian frame, where each node of the computational mesh follows the associated material particle during motion (Donea et al., 2004). Allowing for relatively easy tracking of free surfaces and interfaces but can be weaker when attempting to follow substantial distortions in the computational domain.

The fundamental dilemma of modeling FSI, according to (Richter, 2010), is coupling two systems of partial differential equations expressed in two different coordinate systems. Talking about **coupling** implies a problem in which several components interact **dynamically** and, as mentioned by (Felippa et al., 2001), the physical interaction is multiway. In this case study, for instance, the external environmental forces change the position of the structure, this is the **geometric condition**; the attached fluid moves satisfying the **kinematic condition**; and the change in the fluid-domain results on a flow field alteration, hence generating new (different) forces on the structure, **dynamic condition**. Those three conditions (geometric, kinematic, and dynamic) mainly determine the dynamics of any coupled system (Richter, 2017).

In order to solve the dilemma, one must impose a set of coupling conditions at the interface, where the spatial coordinates of the various systems get mapped. Therefore, one can fully describe the fluid-structure interaction model by satisfying either a velocity or displacement continuity condition. In this sense, the **kinematic condition** requires equal fluid and solid nodal velocities on the moving fluid-solid boundary; it also acts as a no slip condition for the fluid's velocity on the interface. The **dynamic** one specifies stress continuity between the domains; this reflects the Neumann-condition for normal stresses that drive the solid problem. Finally, the **geometric condition** requires equal displacements of the fluid and solid stress tensors. The geometric condition do not reflect a physical material principle but deal with the domain partitioning (Richter, 2010).

Following a brief discussion of these ideas, the precise governing equations, coupling, and boundary conditions employed in the current WSI problem should be clearer.

3.2 GOVERNING EQUATIONS FOR A NEWTONIAN FLUID

The governing equations of uid ow represent mathematical statements of the conservation laws of physics (Versteeg and Malalasekera, 2016), the purpose of this section is to provide a glimpse of the theoretical background behind some of the concepts in uid dynamics, starting from the conservation of mass and momentum.

When analyzing uid ow phenomena, rst, the uid is assumed as a continuum, meaning that its properties are de ned at every point in space. The continuity assumption is justi ed when considering a threshold for the Knudsen number, de ned in Equation 3.1, where the l is the molecular free path (average distance that the molecule would travel in an agitation process), and L represents the characteristic dimension of the uid particle, usually the diameter.

$$K = \frac{l}{L} \tag{3.1}$$

To ensure continuity, $K < 10^{-2}$, which implies that the molecules' free path (average distance) represents less than 10% of the molecules' characteristic dimension. In other words, the assumption is valid only for uids with closely spaced molecules. Which may not always be the case, when considering rare ed liquids, for example, the same no longer holds, as can be seen in the right side of Figure 3.1*.. This is relevant, since the continuity assumption is one of the most important in the study of continuum mechanics, which laid the foundation for what is now known as Computational Fluid Dynamics (CFD).

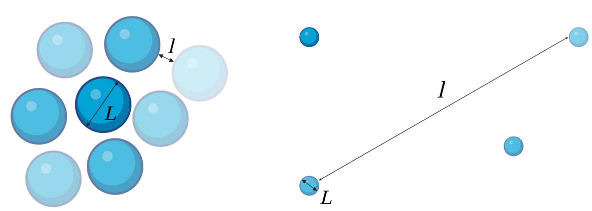

Figure 3.1. Schematic for continuity assumption. Continuous liquid at left, rare ed liquid at right.

Furthermore, within that assumption, uid ow behavior can be categorized as either Newtonian or non-Newtonian. For the problem proposed on this investigation, the author is concerned only in the physics and behavior of Newtonian uids; these are distinguished by the linear relationship between their shear stress/shear rate, and their molecular viscosity ,

*All the schematics used in this thesis have been generated with BioRender.com which measures the ability of a fluid to resist deformation when subjected to inertial forces.

Flows can also be classified mathematically according to the partial differential equations describing them. As will be shown in the following sections, fluid flows are governed by the Navier-Stokes equations, which are nonlinear second-order partial differential equations in four independent variables. In general, flows are unsteady and three dimensional.

3.2.1 SINGLE PHASE NAVIER-STOKES EQUATIONS (NSE)

The system of equations that governs a Newtonian, time-dependent,three dimensional fluid flow are represented in Lagrangian form as:

$$\frac{d\rho}{dt} + \nabla \cdot (\rho \mathbf{u}) = 0 \tag{3.2}$$

$$\frac{d(\rho \mathbf{u})}{dt} = \rho \mathbf{g} + \nabla \cdot \bar{\bar{\tau}} \tag{3.3}$$

Where $\mathbf{u}$ stands for the velocity vector, μ is the dynamic viscosity, ρ the density, $\mathbf{g}$ the gravitational acceleration vector, and $\bar{\bar{\tau}}$ the stress tensor.

Equation 3.2 accounts for a mass balance for the fluid element,

Rate of increase of mass in fluid element = Net rate of flow of mass into fluid element

And Equation 3.3 comes from Newton's second law when applied to the fluid particle,

Rate of increase of momentum of a fluid particle = Sum of the forces on the particle

Furthermore, as indicated by (Buresti, 2015), it is customary to decompose the stress tensor $\bar{\bar{\tau}}$ as in Equation 3.4, where $\bar{\bar{I}}$ is the identity vector and p_e is the equilibrium (or thermodynamic) pressure. When analyzing the expression, one can see that the component $-p_e\bar{\bar{I}}$ is isotropic by construction, and that depends on motion only through the values of density and temperature.

However, the component ${}_v$ represents the viscous stress tensor, and it has a relation with the local velocity of deformation of an elementary volume of uid, which is determined, at rst order, by the tensor $\nabla\mathbf{u}$.

$$\overline{\overline{}} = -p_e\bar{\bar{I}} + {}_v \qquad (3.4)$$

Now, this $\nabla\mathbf{u}$ tensor can be decomposed: On one hand, its symmetric part (or the rate of stress tensor), say $\mathbf{E}$, which characterizes the changes in shape and volume of an elementary volume of uid; and its antisymmetric part on the other hand, say $\boldsymbol{\Omega}$, which describes the rigid rotation of that volume in an elementary time interval. Since, as previously established, this section considers only Newtonian uids, the ${}_v$ is assumed to be independent from $\boldsymbol{\Omega}$, and linearly dependent on $\mathbf{E}$. Then, the most general form of the viscous stress tensor of an homogeneous and isotropic Newtonian uid is given by Equation 3.5,

$${}_v = (\quad \boldsymbol{\nabla}\cdot\mathbf{u})\bar{\bar{I}} + 2 \quad \mathbf{E} \qquad (3.5)$$

Which is where the Stokes' hypothesis comes to play, since he suggested to assume that the two coe cients of viscosity,   and   , are linked by the relation in Equation 3.6.

$$+ \frac{2}{3} \quad = 0 \qquad (3.6)$$

Assuming the validity of that hypothesis is equivalent to state that isotropic dilations of an elementary volume of uid do not produce viscous stresses. In other words, even though the rate of stress tensor, $\mathbf{E}$, is composed in reality by the sum of its isotropic and deviatoric parts, say $\mathbf{E} = \mathbf{A} + \mathbf{D}$, under the Stokes hypothesis one considers only the deviatoric part, arriving at Equation 3.7,

$${}_v = (\quad \boldsymbol{\nabla}\cdot\mathbf{u})\bar{\bar{I}} + 2 \quad \mathbf{D} \qquad (3.7)$$

Where $\mathbf{D}$ is given by,

$$\mathbf{D} = \frac{1}{2}(\boldsymbol{\nabla}\mathbf{u} + \boldsymbol{\nabla}\mathbf{u}^T) \qquad (3.8)$$

Then, when substituting Equation 3.6 and 3.8 on Equation 3.7, the shape of the viscous stress tensor for a Newtonian uid with the Stokes hypothesis is given by Equation 3.9,

$$_v = (-\frac{2}{3} \ \nabla \cdot \mathbf{u})\bar{\bar{I}} + \quad (\nabla \mathbf{u} + \nabla \mathbf{u}^T) \tag{3.9}$$

Furthermore, the Stokes' hypothesisalso implies that the thermodynamic pressurep_e coincides with the mechanical pressure$P$. Considering this, and substituting Equation 3.9 into Equation 3.4 one arrives at the stress tensor given by,

$$\bar{\bar{\ }} = \ -\left(P + \frac{2}{3} \ \nabla \cdot \mathbf{u}\right)\bar{\bar{I}} + \quad (\nabla \mathbf{u} + \nabla \mathbf{u}^T) \tag{3.10}$$

Finally, considering the dynamic pressurep_d, at a position $\mathbf{x}$ and time t,

$$p_d(\mathbf{x}; t) = P(\mathbf{x}; t) - \ (\mathbf{x}; t)\mathbf{g} \cdot \mathbf{x} \tag{3.11}$$

One arrives at the Navier-Stokes equations for a Newtonian, time-dependent,three dimensional uid ow under the Eulerian conservative form,

$$\frac{@}{@t} + \nabla \cdot (\ \mathbf{u}) = 0$$

$$\frac{@(\ \mathbf{u})}{@t} + \nabla \cdot (\ \mathbf{u}\mathbf{u}) = -\nabla p_d - \frac{2}{3}\nabla(\ \nabla \cdot \mathbf{u}) - (\mathbf{g} \cdot \mathbf{x})\nabla \ + \nabla \cdot \left(\ (\nabla \mathbf{u} + \nabla \mathbf{u}^{\mathbf{T}})\right)$$

3.2.2 TWO-PHASE FLOW MODELING AND INTERFACE TREATMENT

There are several numerical approaches to simulate multiphase Newtonian ows. For accurate and stable two-phase ow simulations considering wave propagation, as the ones this thesis is concerned about, the proper free-surface modeling is essential in order to maintain the wave amplitudes, limit dissipative behavior, and avoid instabilities in the ow throughout the simulation. The free-surface modeling must include some type of numerical treatment to account for the discontinuous properties at the interface, and there are three aspects of the interface that must be considered.

First, the **interface capturing**, which refers to the numerical approach chosen to model the phenomena. Among some frequently used approaches one can nd the Volume of Fluid method, (VOF), the Level-set method, and the Phase Function method. Their di erence lies purely in their mathematical formulation and assumptions, and further discussion on their differences can be found in (Kim, 2021). Second, the modeling also requires to consider the algorithms employed for the transport of the free-surface in time. The algorithm, or **interface convection scheme** is dependent on the choice of interface capturing scheme. Details on the different algorithms are out of the scope of this research, but usually one can solve the interface movement either geometrically or algebraically. Finally, the way the properties (physical quantities) are evaluated in the interface cells is often referred to as **interface conditions**. One could chose to consider having two separated fluids, where the interface condition connects them and must be defined as a proper and rigorous boundary condition, ensuring kinematic and dynamic continuity across the free-surface, this is known as the *two-fluids model*; or, one could consider that the interface is defined as one $fluid_1$=$fluid_2$ mixture, the so-called *two-phase single field* condition. In that case, a function must be defined so that continuity of velocity and stress can be ensured through a smooth transition between both phases, much like calculating the physical properties, or fields, as a blend between the same properties of each individual phase. In summary, to account for the discontinuities present at the free surface, the employed numerical treatment must take into account the discrete representation of the boundary, its evolution in time, and the special considerations when trying to impose boundary conditions on it.

3.2.3 TWO-PHASE SINGLE-FIELD NSE

In this thesis, the single Volume Of Fluid (VOF) method shall be considered. The BGF simulations are expected to render large deformations on the free boundaries free surface–, therefore, the Eulerian coordinate representation has advantages compared with Lagrangian one, as discussed by (Hirt and Nichols, 1981). The principle behind the method lies on the concept of **volume fraction**: if one defines a function whose value is unity at any point occupied by fluid, and zero otherwise, the average function value in a particular cell would represent the fractional volume of the cell that is occupied by fluid. In this sense, the cells reporting values between zero and one contain a free surface. If the boundary normal-outward component and the function value are known, a line cutting the cell can be constructed to approximate the interface, the later can then be used for setting boundary conditions.

For a two-phase water-air flow, the phase indicator function is defined as = 1 for a cell filled with water, and = 0 for cells immersed in the air phase. Then, the interface between both phases is a continuous transition zone with 0 < < 1. Here, the averaged local density as well as the averaged kinematic and dynamic viscosity (,) are defined as in Equations 3.12 to 3.14, where the subscripts 'w' and 'a' refer to water and air, respectively.

$$= \; _w + (1 - \;) \; _a \tag{3.12}$$

$$= \; _w + (1 - \;) \; _a \tag{3.13}$$

$$= - \tag{3.14}$$

As above-mentioned, when modeling single-phase uid ow one must account for the mass balance, expressed by the continuity equation, and a force balance from which the momentum equation is derived. Now that the model extends to consider two-phase ows, one must also account for a governing equation for the phase indicator function . First, let's start by discussing the changes in the continuity equation. Since now there are two phases one arrives at two continuity equations, written in Eulerian form as,

$$\frac{@(\; _w)}{@t} + \nabla \cdot (\; _w \mathbf{u}) = 0 \tag{3.15}$$

$$\frac{@([1 - \;] \; _a)}{@t} + \nabla \cdot ([1 - \;] \; _a \mathbf{u}) = 0 \tag{3.16}$$

Where the velocity of air and water are assumed to be equal in transition zones ($\mathbf{u}$), as part of the two-phase single eld approach. However, considering both the air and water phases as incompressible ows (the density variation due to the pressure di erence is neglected), and after some algebraic manipulation one arrives at the continuity expression given by,

$$\nabla \cdot \mathbf{u} = 0$$

Second, the governing equation of the phase indicator function is also derived from the mass conservation principle, expressed by Equation 3.17 when considering any control volume V.

$$\frac{d}{dt} \int_V \; dV = 0 \tag{3.17}$$

Where, if applied the Reynolds transport theorem, the expression is equivalent to,

$$\frac{d}{dt} \int_V \; dV = \int_V \left(\frac{@}{@t} + \nabla \cdot (\; \mathbf{u}) \right) dV = 0 \tag{3.18}$$

Now, if one applies the vector identity to the $[\nabla \cdot (\; \mathbf{u})]$ component, one can re-write the inner term of the volume integral as in Equation 3.19.

$$\frac{\partial}{\partial t} + \nabla \cdot (\ \mathbf{u}) = \frac{\partial}{\partial t} + \mathbf{u} \cdot \nabla \ + \ \nabla \cdot \mathbf{u} = 0 \tag{3.19}$$

Finally, when considering the current de nition of density, given by Equation 3.12, one arrives at the transport equation of the phase fraction under the incompressible assumption as,

$$\frac{\partial}{\partial t} + \nabla \cdot (\ \mathbf{u}) = 0$$

And third, considering the formulation of and , the momentum equation can be written as,

$$\frac{\partial \ \mathbf{u})}{\partial t} + \nabla \cdot (\ \mathbf{u}\mathbf{u}) = -\nabla p_d - (\mathbf{g} \cdot \mathbf{x})\nabla \ + \nabla \cdot (\ \nabla \mathbf{u}) + \nabla \ \cdot \nabla \mathbf{u}^{\mathbf{T}} + \ _k \nabla$$

Where $\mathbf{u}$ is the continuous uid velocity eld; is the averaged density eld; $\mathbf{g}$ is the gravitational eld vector; $\mathbf{x}$ is the position vector from reference to cell center; p_d is the dynamic pressure; and the term [$_k\nabla$] accounts for the surface tension on the interface between water and air, which will be considered negligible in this thesis. The values considered for the uids' properties are listed in Table 3.1.

Density		**Unit**
$_w$	1000	kg=m^3
$_a$	1:225	kg=m^3
Linear viscosity		
$_w$	10^{-3}	Ns=m^2
$_a$	10^{-5}	Ns=m^2

Table 3.1. Physical quantities considered for two-phase ow simulations.

It is important to notice that usually the Navier-Stokes equations are re-written under the assumption that the e ective dynamic viscosity ($_{eff}$) can be approximated—or averaged— as a summation of linear viscosity ($_l$) and eddy or turbulent viscosity ($_t$), where the latter is calculated from the chosen turbulence model. This approximation is called Reynolds Averaged Navier-Stokes Equations (RANSE), since it uses the Reynolds statistical decomposition to re-write the equations. However, for the rst instances of this research, the turbulence e ects are neglected and the simulations performed under the \laminar" turbulence model. This is a big assumption but justi ed under the premise that, in the BGF case, many other variables are rst to be veri ed and validated before going into the turbulence modeling discussion.

3.2.3.1 Artificial interface compression technique

As mentioned before, the two-phase single field approach considers the velocity of air and water to be equal in the transition zones. However, as mentioned by (Rusche, 2002) this assumption is prone to problems associated with the convection of a step function. Henry Weller, architect and principal developer of OpenFOAM, proposed an interface compression scheme based on counter-gradient transport to maintain sharp interfaces during a VOF simulation (Greenshields, 2020). He found that the necessary compression of the interface is not achieved by using a compressive differencing scheme, but rather by introducing an extra, artificial compression term into the phase function field that would help in minimizing the smearing of the transition zone of the interface. Then, the relative velocity between air and water at the interface is defined as,

$$\mathbf{u_r} = C_\alpha (u_w - u_a) \tag{3.20}$$

And, the compression term is given by Equation 3.21,

$$\mathbf{u_{comp}} = (1 - \alpha)\alpha\,\mathbf{u_r} \tag{3.21}$$

Finally, the governing equations for the artificially compressed two-phase single-field VOF are given by,

$$\frac{\partial \rho}{\partial t} + \nabla \cdot (\rho\mathbf{u} + [(\rho_w - \rho_a)\mathbf{u_{comp}}]) = 0$$
$$\frac{\partial \alpha}{\partial t} + \nabla \cdot (\alpha\mathbf{u}) + \nabla \cdot \mathbf{u_{comp}} = 0$$
$$\frac{\partial \rho\mathbf{u})}{\partial t} + \nabla \cdot (\rho\mathbf{u}\mathbf{u} + (\rho_w - \rho_a)\mathbf{u_{comp}}\mathbf{u}) = -\nabla p_d - (\mathbf{g}\cdot\mathbf{x})\nabla\rho + \nabla \cdot (\mu\nabla\mathbf{u}) + \nabla\mu \cdot \nabla\mathbf{u}^{\mathbf{T}}$$

3.2.4 TWO-PHASE SINGLE-FIELD NSE WITH A MOVING REFERENTIAL

To account for rectilinear motion with respect to the Galilean earth frame of reference, the equations can be re-written in a moving-domain frame with velocity $\mathbf{v}_0$ and acceleration $\mathbf{a}_{cc_0}$. Under this moving-frame the mass conservation and phase transport equation maintain the aforementioned formulation; however, the acceleration from the moving-domain regarding the xed-domain is accounted for in the momentum equation in which an additional term appears,

$$\frac{\partial(\mathbf{u})}{\partial t} + \nabla\cdot(\mathbf{uu} + (_{w} - _{a})\mathbf{u_{comp}}\mathbf{u}) = -\nabla p_{d} - (\mathbf{g}\cdot\mathbf{x})\nabla + \nabla\cdot(\nabla\mathbf{u}) + \nabla \cdot\nabla\mathbf{u}^{\mathbf{T}} - \mathbf{a}_{cc_0}$$

This moving-domain-reference-frame consideration has been implemented in foamStar, since it is convenient for naval and ocean engineering applications where the movement of the body is one of the important variables to account for and analyze.

3.3 WAVE-STRUCTURE INTERACTIONS

The equations described in Section 3.2 account only for the fluid dynamics. However, as noted in section 3.1, the simulations in this thesis must also solve for the solid dynamics of the moving body. In this sense, this section describes the additional boundaries defined around the fluid domain and the mathematical considerations for modeling rigid body motions in a WSI simulation.

3.3.1 BOUNDARY CONDITIONS

The Dirichlet and Neumann boundary conditions (BCs) are the most commonly used. The Neumann boundary condition imposes flux values (gradient of the field normal to the boundary), and the Dirichlet condition sets a priori known values for generic scalar or vector fields. OpenFOAM considers "physical" boundary conditions. They are more concerned with identifying the physics of the problem and adequately reproducing it in the simulation setting than with providing an exact fixed scalar, vector, or flux value. These physical boundary conditions can include or combine the Dirichlet and Neumann types. In order to solve the Navier-Stokes equations above-mentioned, one must define proper boundary conditions for the velocity $\mathbf{u}$, the dynamic pressure p_d, and the phase function field . Figure 3.2 illustrates an example of the five boundaries usually defined in a two-phase computational simulation, namely: inlet, outlet, bottom, top, and the floating body. Their modeling assumptions will be addressed in subsequent sections.

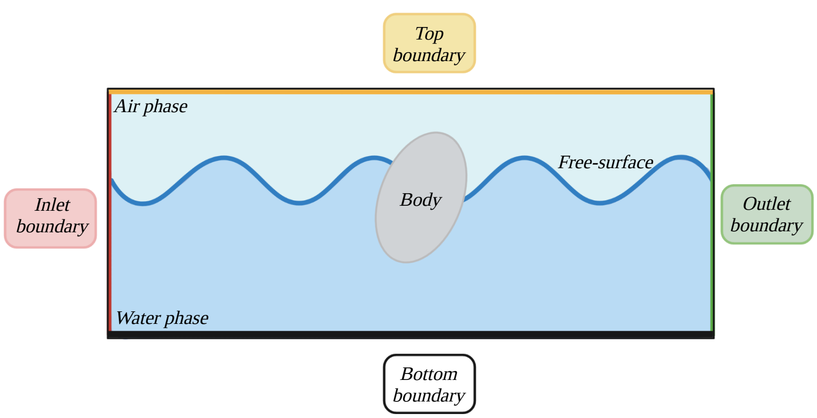

Figure 3.2. General boundary conditions schematic for two-phase numerical simulations.

3.3.1.1 Velocity

In naval or ocean engineering applications, one must be able to model boundaries such as solid bodies or walls. To that aim, this thesis considers the assumption that the uid particles adhere themselves to such physical non-porous boundaries; this translates to a no-slip BC, and it is imposed on the body/wall, forcing the uid velocity as the local body/wall velocity. Considering the later to be $\mathbf{u}_{wall}$, the no-slip Dirichlet boundary condition reads as:

$$\mathbf{u} = \mathbf{u_{wall}} \tag{3.22}$$

Regarding the inlet and outlet boundaries of the computational domain, the velocity values are explicitly given to the model, dictated initially by the imposed wave pro le, and handled posteriorly by the relaxation zones and schemes discussed in subsequent sections.

3.3.1.2 Dynamic pressure

Typically, the Neumann-type dynamic pressure boundary condition determines the ux, which in the context of transport phenomena refers to the rate-of- ow of a property per unit area, citeMoukalled2016. When imposed on a partial di erential equation, such as Equation 3.2.3, the condition speci es the values of the gradient of the dynamic pressure eld applied at a boundary. Mathematically, and assuming that any xed or moving boundary is given implicitly as the set of points $(x; y; z)$ satisfying $F(x; y; z; t) = 0$, the gradient can be expressed by a normal-vector at any point on such boundary. Therefore, the rst step to derive the dynamic pressure BC is to apply the dot product of the momentum equation with a surface unit normal-vector $\mathbf{n}$, as in Equation 3.23.

$$\frac{D(\ \mathbf{u})}{Dt} \cdot \mathbf{n} = -\mathbf{n} \cdot \boldsymbol{\nabla} p_d - (\mathbf{g} \cdot \mathbf{x}) \boldsymbol{\nabla} \ \cdot \mathbf{n} + \mathbf{n} \cdot \boldsymbol{\nabla} \cdot \left(\ (\boldsymbol{\nabla} \mathbf{u} + \boldsymbol{\nabla} \mathbf{u}^{\mathbf{T}}) \right) \tag{3.23}$$

The left-hand side term expresses the time rate of change (material derivative) of the momentum of the ow (the product between its mass and velocity). The right-hand side terms represent the surface-normal gradient for dynamic pressure, density, and shear stress. The second step in deriving the BC is to apply the same logic for all boundaries that already consider the Dirichlet velocity BC and re-write the equation in terms of the dynamic pressure as:

$$\mathbf{n} \cdot \nabla p_d = -\frac{D(\rho \mathbf{u_{wall}})}{Dt} \cdot \mathbf{n} + \mathbf{n} \cdot \nabla \cdot \left(\mu (\nabla \mathbf{u_{wall}} + \nabla \mathbf{u_{wall}^T}) \right) - (\mathbf{g} \cdot \mathbf{x}) \nabla \rho \cdot \mathbf{n} \tag{3.24}$$

Finally, considering $\mathbf{x}$ to be near the free surface (it is the only region where the surface-normal gradient of density is different from zero), the final expression for the dynamic pressure BC for an incompressible two-phase flow simulation is given by:

$$\frac{\partial p_d}{\partial n} = -\frac{D(\rho \mathbf{u_{wall}})}{Dt} \cdot \mathbf{n} + \mathbf{n} \cdot \nabla \cdot \left(\mu (\nabla \mathbf{u_{wall}} + \nabla \mathbf{u_{wall}^T}) \right) - (\mathbf{g} \cdot \mathbf{x}) \frac{\partial \rho}{\partial n} \tag{3.25}$$

3.3.1.3 Phase fraction

The fluid's velocity passively transports the phase function, as evident from Equation 3.2.3. As a result, there is no need for precise phase function values on the body/wall boundaries. However, for the free-surface boundary condition, wave elevation values are explicitly imposed at the inlet and outlet boundaries of the domain.

3.4 WAVE THEORY

Throughout this thesis, the interaction between waves and structure has been repeatedly mentioned as the main focus of study when designing or optimizing platforms subjected to oceanic conditions. Previous sections have addressed the mathematical models that describe fluid and solid dynamics. This section focuses on the description of the wave modeling mathematical background. The relevance of this topic lies in acknowledging that the quality of the generated numerical waves is essential for accurate WSI simulations, but also since previous research concluded that wave loads dominate the platform motions in the BGF case study (Li et al., 2020).

3.4.1 CHARACTERISTICS OF WAVES

As explained by (Dalrymple, 1991), the key characteristics to describe any wave include the length, height, amplitude, and depth of the water across which the wave is propagating. Theoretically, all other parameters, including wave-induced water velocities and accelerations, may be derived from these values. One can also notice the parameter, which refers to the wave —or free surface— elevation. As noted by (Boccotti, 2015), The function (x) at a fixed instant represents the wave on the **space domain**, depicted in Figure 3.3, (a). But, recording the surface elevation at a fixed point, as (t), gives the wave on the **time domain**, as in Figure 3.3, (b).

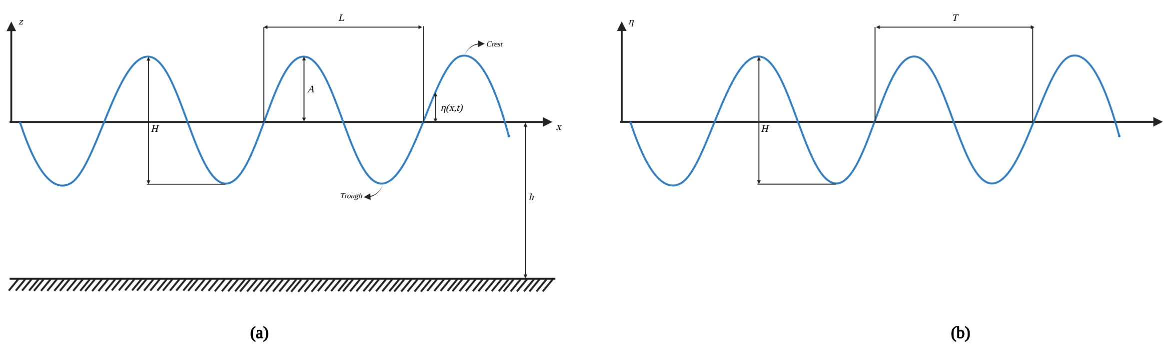

Figure 3.3. Two-dimensional wave schamatic. (a) Wave on the space domain. (b) Wave on the time domain.

Let us define some of the parameters seen in the previous figure. The highest elevation on the wave is the crest, while the lowest is the trough. These points also define the wave amplitude A. The vertical distance between the crest and trough defines the wave height H. The wavelength L or refers to the interval between one zero up-crossing and the next, and it is a measure in the space domain. The period T is de ned by the same distance but evaluated in the time domain. Furthermore, analyzing the spatial domain representation, it is relevant to notice that the coordinate axis used to describe the wave propagation (x for this schematic) is located at the \still-water line", given by $z = 0$. Therefore, the bottom boundary lies at $z = -h$.

Other relevant variables derive from these parameters. As the wave propagates a distance L in time T, one can de ne the speed at which the same is traveling as $c = \frac{L}{T}$, and it is called celerity. The wave amplitude results from $A = \frac{H}{2}$. The angular frequency, by de nition, is $! = \frac{2\pi}{T}$. And the \wave number"is given by $k = \frac{2\pi}{L}$.

Furthermore, considering the wave propagation as part of a circular motion, as in Figure 3.4, it is possible to introduce two additional parameters: the wave steepness and the dispersion parameter. From Figure 3.4, (a), one can infer that $y = r \sin$. Analogously, the blue line in Figure 3.4, (b) shows a wave depiction with a slight asymmetry, more \wavey-looking". In that sense, a rst approximation would be to consider that the wave follows a sinusoidal trend given by $(x; t) = A \sin$, with a wavelength that will depend on the water depth, and the wave period, this constitutes the assumption of harmonic-type-waves, described by the linear or \airy wave"model.

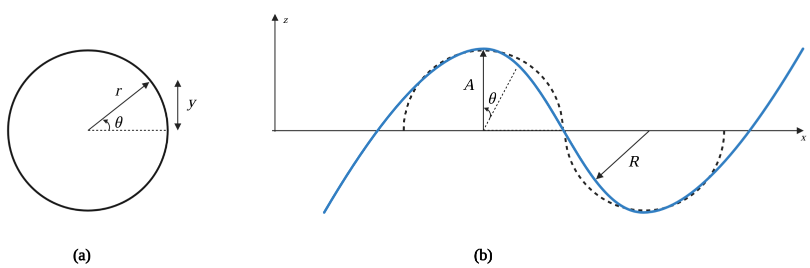

Figure 3.4. Wave description considering a circular orbit.

However, waves do not appear or propagate in this perfectly rounded shape when in nature. The wave steepness parameter characterizes the nonlinearity of the waveand how far it is from the linear circular orbit — . It expresses the ratio between the wave height and the wavelength. Having a very high crest or a small wavelength (see Figure 3.5, (a)) results in steeped waves—or highly nonlinear—. Moreover, one can model waves using the linear model when having small crested waves and vast wavelengths (Figure 3.5, (b)).

Note that the wave steepness is de ned mathematically as:

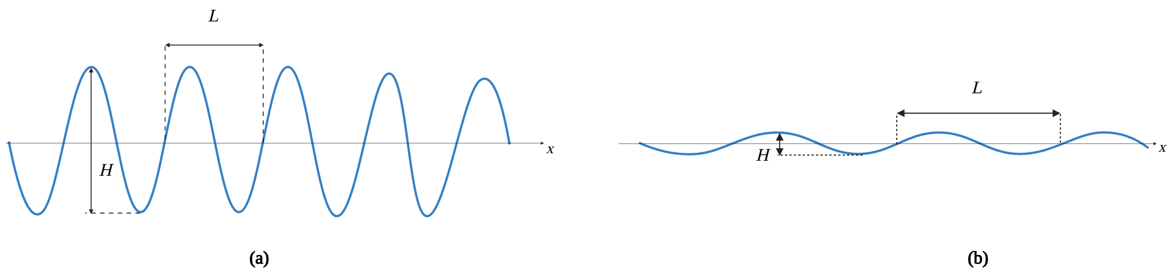

Figure 3.5. Wave steepness, or nonlinearity. (a) Highly non-linear wave. (b) Airy or linear wave.

$$\varepsilon = \frac{H}{L} = \frac{2\ A}{L} = kA \tag{3.26}$$

The dispersion parameter relates the wave number and the water depth. It is given by:

$$= kh \tag{3.27}$$

If one analyzes a wave propagating with a **fixed wavelength**, it will travel faster as the water depth increases, as opposed to a slower propagation rate for shallower waters. Furthermore, the dispersion relation links space and time: if one analyzes waves propagating at a **fixed water depth**, the waves will propagate faster as the wavelength increases. The dispersion relation enables the calculation of the phase velocity c and group velocity c_g of the wave as a function of frequency.

These parameters and considerations have proven that the linear wave theory can be reasonably accurate for some purposes, and it is especially advantageous for its ease of use. However, when designing structures that can safely withstand rough sea conditions, the degree of randomness in the ocean waves must be accounted for. With that goal, researchers have developed more complicated nonlinear wave theories. The higher-order spectral (HOS) model employed in this thesis is one of them.

3.4.2 REGULAR AND IRREGULAR WAVES

Two distinct types of waves —regular and irregular— can be explored within the context of wave modeling. It is relevant to address the difference between these two since this research aims to analyze the influence of both models on the response of the BGF structure.

A regular wave progresses steadily and periodically. Since it has only one frequency component, it is also known as monochromatic wave. The term "monochromatic" derives from the analogy of water waves to light waves and the relation of color to frequency. (Dalrymple, 1991). In this sense, the free-surface elevation values vary as a sinusoidal function of time and distance. However, by analyzing the actual sea surface, one can see that many different waves are moving in various directions, each with a different frequency, phase, and amplitude. They all interact among themselves, which results in more waves. The irregular wave models try to render a more realistic description of the sea states by including various wavelengths or wave frequencies.

Figure 3.6 highlights the difference between regular (a) and irregular waves (b)[*]. On top, it depicts the free-surface elevation in the **time domain**, and at the bottom, the wave description on the **frequency domain**. Here, the ordinate axis shows the variance spectral density S, a pseudo-energy measure. The energy would be $E = g\frac{A^2}{2}$, while $S = \frac{A^2}{2}$, so it is not consistent with energy units. Nonetheless, this variance density is used in the ocean engineering context to show the wave energy distribution as a function of frequency for a sea state.

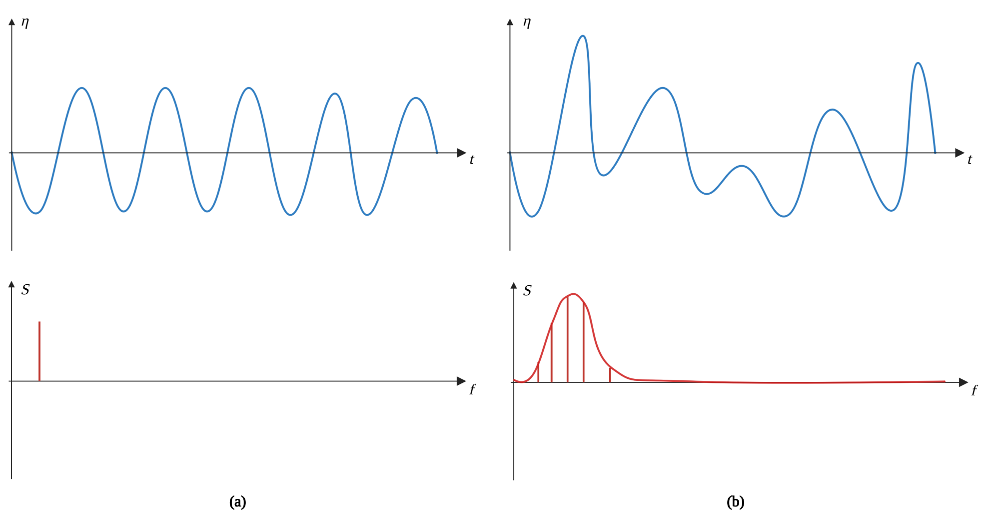

Figure 3.6. Wave representation in the frequency domain. (a) Regular wave. (b) Irregular wave.

[*]The illustration depicts the distinction between regular and irregular waves. It does not represent the actual energy content or a true measurement result.

3.4.3 DISPERSIVE WAVES

Di erent wave types are present in the ocean: sound, capillary, gravity, internal, and planetary waves (Massel, 2017). As mentioned before, they all coexist and interact in a way that the oceans' free-surface response enclosures a broad range of wavelengths and periods, from capillary waves, with periods of less than a second, to tidal oscillations with periods of the order of days, and everything in between (See Figure 3.7)[†].

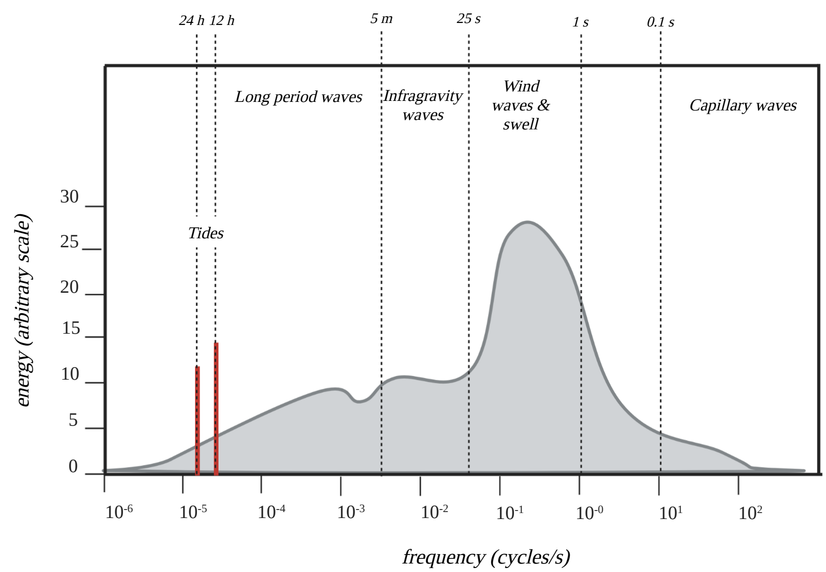

Figure 3.7. Schematic of oceans' energy distribution as function of frequency.

This thesis examines waves over periods comparable to those of wind-induced waves. When they occur in the ocean, they are also known as gravity waves because they arise from gravity forces acting on water particles displaced from equilibrium at the ocean surface. Furthermore, various wave types require distinct modeling approaches and procedures. The waves under consideration in this thesis are called dispersive, and all methods devised to represent them assume that the dispersion parameter is not tiny.

$$= kh \geq O(1)$$
$$\therefore \quad \gtrapprox 0{:}3$$

[†]The image conveys a sense of the relative importance of various types of surface oscillations, but it may not always reflect the real energy content.

Figure 3.8 presents a schematic of some of the most common wave-modeling methods used for dispersive waves.

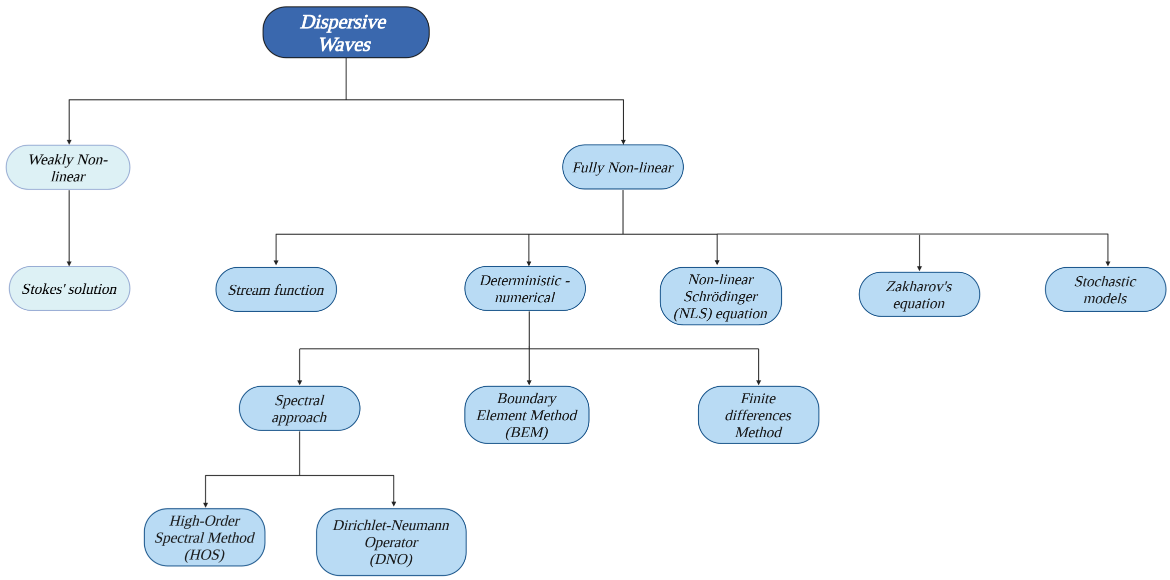

Figure 3.8. Wave models for dispersive waves.

The author acknowledges that, for regular waves, the most used model is the \Stream-function" one, introduced in (Rienecker and Fenton, 1981). However, the HOS model has been chosen in this thesis to model both regular and irregular waves. The HOS-NWT solver developed in LHEEA Lab (ECN/CNRS) enables the de nition of a ramp at the beginning of the numerical wave, and this goes in better accordance with the waves produced on the experimental campaign since it takes some time for the wave-maker to generate waves with a certain speci ed amplitude. The solver has been used to simulate regular waves for the validation described in (Ducrozet, 2007), and the thesis of (Choi, 2019).

3.4.4 HIGH ORDER SPECTRAL (HOS) MODEL

The high-order spectral model was initially developed by (West et al., 1987) and (Dommermuth and Yue, 1987). Since then, several authors have employed and veri ed HOS models to examine various physical phenomena, such as nonlinear energy transfers, modulational instabilities, bimodal seas, and freak waves. As a result, this approach may be deemed mature and applicable to actual engineering applications (Ducrozet et al., 2016). The method enables the fully nonlinear simulation of gravity-wave evolution within periodic, unbounded 3D domains. In comparison with classical time-domain models such as the BEM, this spectral approach presents the two assets of its fast convergence and its high computational efficiency (employing FFTs), allowing it to accurately simulate long-time 3D sea-state evolutions with fine meshes (Ducrozet et al., 2007).

The problem considers a rectangular fluid domain D with constant water depth associated with a fixed Galilean reference frame. The origin lies at one corner of the domain, with the vertical axis oriented upward and $z = 0$ at the mean free surface. The equations follow the potential flow theory, which implies that the fluid is incompressible and inviscid, besides the flow being considered irrotational. Such assumptions allow the definition of the potential $\phi(x, y, z, t)$ given by:

$$\mathbf{u}(x, y, z, t) = \nabla\phi \tag{3.28}$$

With the assumption of irrotational motion and an incompressible fluid, the velocity potential should satisfy the continuity equation,

$$\nabla \cdot \mathbf{u} = 0 \tag{3.29}$$

Or,

$$\nabla \cdot \nabla\phi = 0 \tag{3.30}$$

Then, since the divergence of a gradient leads to the Laplace equation, the continuity equation reduces to Equation 3.31 for the velocity potential ϕ:

$$\nabla^2\phi + \frac{\partial^2\phi}{\partial z^2} = 0 \text{ in } D \tag{3.31}$$

Defining the free-surface elevation function $\eta(x, y, t)$ in the fixed reference frame, one arrives at the free surface boundary conditions. At any boundary, the fluid velocities must satisfy certain physical restraints. These on the water-particle kinematics give rise to the kinematic boundary conditions. The most obvious one is that if one defines a fluid interface, there must be no flow across it —wouldn't be much of an interface if there were flow through it—. The kinematic BC is in Equation 3.32, and (Dalrymple, 1991) gives additional details on its development.

$$\frac{\partial \eta}{\partial t} = \frac{\partial \phi}{\partial z} - \frac{\partial \phi}{\partial x}\frac{\partial \eta}{\partial x} - \frac{\partial \phi}{\partial y}\frac{\partial \eta}{\partial y} \tag{3.32}$$

On the other hand, the dynamic free surface boundary condition requires that the pressure on the free surface remains uniform along the wave propagation. Such a condition reads as:

$$\frac{\partial \phi}{\partial t} = -g\eta - \frac{1}{2}\nabla \phi^2 \tag{3.33}$$

The HOS method defines the following 2D field:

$$\tilde{\phi}(x;y;t) = \phi(x;y;\eta(x;y;t);t) \tag{3.34}$$

and noting W the vertical velocity at the free surface:

$$W(x;y;t) = \frac{\partial \phi}{\partial z}(x;y=\eta;t) \tag{3.35}$$

With these notations, the free surface boundary conditions may be rewritten as follows:

$$\frac{\partial \eta}{\partial t} = \left(1 + \frac{\partial \eta^2}{\partial x} + \frac{\partial \eta^2}{\partial y}\right) W - \frac{\partial \tilde{\phi}}{\partial x}\frac{\partial \eta}{\partial x} - \frac{\partial \eta}{\partial y}\frac{\partial \tilde{\phi}}{\partial y} \tag{3.36}$$

$$\frac{\partial \tilde{\phi}}{\partial t} = -g\eta - \frac{1}{2}\nabla \tilde{\phi}^2 + \frac{1}{2}\left(1 + \frac{\partial \eta^2}{\partial x} + \frac{\partial \eta^2}{\partial y}\right) W^2 \tag{3.37}$$

Equivalently, in a more compact notation,

$$\frac{\partial \eta}{\partial t} = (1 + |\nabla \eta|^2)W - \nabla \tilde{\phi} \cdot \nabla \eta$$
$$\frac{\partial \tilde{\phi}}{\partial t} = -g\eta - \frac{1}{2}|\nabla \tilde{\phi}|^2 + (1 + |\nabla \eta|^2)W^2$$

The premise of Fourier analysis follows from the fact that any piecewise continuous function (periodic over time) can be represented over an interval of time as a sum of sines and cosines or in an exponential complex series when combining the Fourier principle with the Euler identities. Following the HOS procedure, surface quantities η and $\tilde{\phi}$ are expressed on a spectral basis to enable the use of Fast Fourier Transforms (See Equations 3.38 and 3.39). Where $k_m = m \Delta k_x = m \frac{2\pi}{L_x}$ represent the wave-numbers and L_x the horizontal dimension of the domain D.

$$\eta(x;t) = \sum_m B_m^{\eta}(t) \exp(i k_m x) \tag{3.38}$$

$$\tilde{\phi}(x;t) = \sum_m B_m^{\tilde{\phi}}(t) \exp(i k_m x) \tag{3.39}$$

After knowing the surface quantities η and $\tilde{\phi}$, the HOS procedure moves onto evaluating the vertical velocity at the free-surface $W(x;t)$ through a Taylor series expansion in wave steepness ε up to the so-called HOS order M. In this way, the original Dirichlet problem for the velocity potential $\Phi(x;z;t)$ on $z = \eta(x;t)$ is transformed into M Dirichlet problems for $\phi^{(m)}(x;z;t)$ on $z = 0$. Furthermore, the vertical velocity W undergoes another Taylor expansion to reach another triangular system for $W^{(m)}$ that is solved iteratively. (Ducrozet et al., 2016) reports further details on the HOS scheme.

3.5 NUMERICAL WAVE GENERATION

Numerical wave tanks (NWT) rely on specific mathematical models to simulate realistic wave conditions, properly propagate the waves throughout the domain, and absorb the reflected waves at the borders. A material wave tank for hydrodynamics and ocean engineering studies usually accounts for the wave generation through wave-makers and an absorption beach at the end to avoid wave reflections that would impair the data acquisition and validity. However, reproducing a wave-maker using moving mesh techniques or a wave-absorption beach in an NWT is computationally expensive and thus often replaced by numerical wave generation and absorption models (Li et al., 2019). Two wave-modeling approaches, the Relaxation Zone method, and the HOS method, are combined in this study.

3.5.1 RELAXATION ZONES (RZ)

The method was initially introduced by (Mayer et al., 1998) as "A fractional step method for unsteady free-surface flow", and its implementation was limited to the wave-absorption by setting the incident outlet solution to zero. Posteriorly, it was extended to account for wave generation in the work of (Jacobsen et al., 2012), which expanded the OpenFOAM code to include the wave relaxation zones into the already existing RANSE-VOF method for free-surface solving. Under this formulation, one can combine the RZs and wave-generating and absorbing boundary conditions. Today, it is one of the most used wave-generation methods by the ocean and coastal engineering community.

The method uses a zone spatially close to the outside boundaries of the numerical domain, where the approach blends the numerical solution to a reference solution using a spatially varying weight function. The zones near the domain boundaries are called relaxation zones (RZ) and are defined using a prescribed length into the domain (See Figure 3.9).

The relaxed fields inside the RZs are computed as a linear combination given by:

$$\phi_r = \omega\, \phi_I + (1 - \omega)\, \phi \tag{3.40}$$

$$\mathbf{u_r} = \omega\, \mathbf{u_I} + (1 - \omega)\, \mathbf{u} \tag{3.41}$$

Where the subscript I denotes the incident wave imposed values, the subscript r refers to the relaxed values, and the rest of the variables correspond to the CFD solutions.

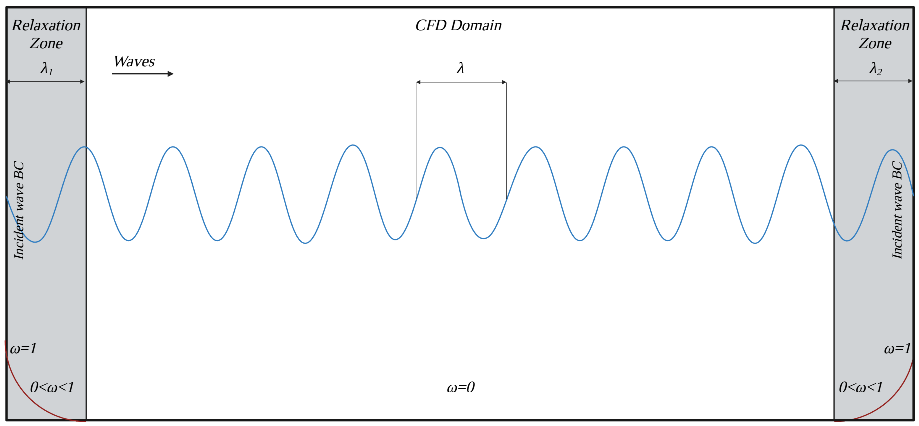

Figure 3.9. Relaxation zone (RZ) method;

Once reached a converged solution the blending procedure is repeated at the end of each time step. The further simulation then takes advantage of the relaxed values. The method prevents waves from being reflected into the domain and allows for numerical waves outside the RZs. The relaxation zone's smooth function ranges between 0 and 1 as a space-dependent weight omega. In foamStar, the default definition of ω is an exponential function given by:

$$\omega(\xi_r) = \frac{e^{\xi_r^{3.5}} - 1}{e - 1} \tag{3.42}$$

Where $\xi_r \in [0;1]$ is the normalized coordinate in the RZ defined as the distance to the boundary divided by the length of the RZ.

3.5.2 HOS-NWT

This study focuses on the simulation of NWT and the generation of the incident wave field for regular and irregular waves using the HOS-NWT solver. The solver applies a pseudo-spectral method to simulate 3D waves with fully non-linear free surface boundary conditions on a periodic domain, besides wave-maker modeling up to third-order. The main characteristics of the HOST (HOS Tank) lie in the presence of a wave-maker and numerical beach. Which, mathematically, represents additional boundary conditions. Furthermore, to model the wave generation by a wave-maker, the potential ϕ, solution of the total problem, is decomposed into $\phi = \phi_{spec} + \phi_{add}$. Where, ϕ_{spec} describes the wave evolution in the fixed reference frame with its free surface, and ϕ_{add} accounts for the wave-maker satisfying the additional boundary conditions. The description of such conditions lies outside this thesis' topic, but the reader is encouraged to review the complete model description in (Ducrozet et al., 2012) and (Choi, 2019).

Employing the HOS methodology described above, one can find the solution after introducing the additional potential. The free surface grid is first discretized and equally spaced to apply inverse FFTs. Then, the reconstruction of the wave fields is necessary to accurately deliver flow quantities to the viscous flow (CFD) model. In this sense, the in-house LHEEA development called Grid2Grid applies inverse FFTs and a quick B-spline module to reconstruct the non-linear wave fields for any arbitrary CFD simulation with any specific time and space discretization. In summary, the rectilinear grid used for the interpolation does not change with time, and the moving CFD receives the results from the B-spline interpolation scheme in space and time. Then again, the details of the Grid2Grid wrapper are not explicitly given in this thesis, but (Choi et al., 2017) and (Li et al., 2021) provide additional information.

Chapter 4

Numerical Methods

This chapter discusses the numerical implementation of the set of equations and mathematical models presented before. The discussion centers around the numerical models implemented for the Computational Fluid Dynamics (CFD) simulations. CFD is a ramification derived from fluid mechanics theory that exploits advances in computing technology to bridge the gap between theoretical and experimental fluid dynamics. The principle is to solve the fluid-flow (or FSI in this case) problem with iterative computations when replacing the governing equations with mathematical models. Such models integrate discretized algebraic expressions over each control volume in agreement with the Finite Volume Method (FVM) approach.

The layout of this chapter is as follows. The first section presents the FVM's general considerations and assumptions, followed by a discussion on temporal and spatial discretization concepts when considering generic equations for the fluid flow problem. The last section describes the numerical models implemented in OpenFOAM and foamStar to simulate WSI cases relevant to this thesis. The final section presents a description of the adopted numerical schemes and the depiction of the implemented algorithm.

4.1 FINITE VOLUME METHOD

This section explains the Finite Volume methodology for generic uid- ow phenomena. The author regards the discussion as a starting point for the method's comprehension before expanding the concepts to the problem in the WSI context.

The general transport Equation (4.1) is obtained when introducing the generic variable . The transport equation is used as a starting point for computational procedures in the FVM, as indicated by (Versteeg and Malalasekera, 2016). This equation has transient, convection, di usion, and source terms, and each brings a characteristic contribution to the equation that needs to be reproduced by the discretization procedure (F. Moukalled, 2016).

The fundamental step of the method relies on the integration of the Equation 4.1 over a three-dimensional control volume CV to yield a discretized equation at its nodal point P, (Equation 4.2). The method began with the one-dimensional steady-state di usion equation, which is the foundational transport process of all. Extension to two and three-dimensional convection-di usion problems followed.

$$\left[\frac{\partial}{\partial t} + \nabla\cdot(\ \mathbf{u})\right] = \nabla\cdot(\ \nabla\ ) + S_{\phi} \tag{4.1}$$

$$\left[\int_{V_P}\frac{\partial}{\partial t}dV + \int_{V_P}\nabla\cdot(\ \mathbf{u})dV - \int_{V_P}\nabla\cdot(\ \nabla\ )dV\right] = \int_{V_P}S_{\phi}dV \tag{4.2}$$

After dividing the domain into a nite number of arbitrary cells, the initially computed values lie inside each control volume. The elements must be convex, and their faces planar. As one wants to solve the general transport equation for the transported quantity in the domain, there must be discernment between internal control volumes and those lying on the boundaries. On that note, one remark is that the FVM makes it truly simple to implement a variety of boundary conditions in a noninvasive manner since the unknown variables are evaluated at the centroids of the volume elements, not at their boundary faces (F. Moukalled, 2016).

The mean values of all variables are computed and stored in the centroid of each control volume. The next step is to convert the volume integrals into surface ones using the Gauss theorem, and the problem reduces to interpolating the cell-centered values (known quantities) to the face centers. After integrating, one arrives at the semidiscrete Equation 4.3. Where $S_f\cdot(\ \mathbf{u}\ )$ is the convective ux and $S_f\cdot(\ \ _{\phi}\nabla\cdot\ \ )$ is the di usive ux.

$$\int_{V_P} \frac{\partial}{\partial t} dV + \sum_f S_f \cdot (\ \mathbf{u}\ )_f - \sum_f S_f \cdot (\quad_\phi \boldsymbol{\nabla} \cdot \ )_f = S_c V_P + S_p V_P \ _P \tag{4.3}$$

The interpolation procedure must render the values at both sides of face f. It is imperative to notice that diffusion affects the distribution of a transported quantity along its gradients in all directions, whereas convection influences it only in the flow direction. Hence, besides computing the transported on the control volume faces, one must also obtain the convective flux across the boundaries (Versteeg and Malalasekera, 2016).

The spatial discretization of the solution domain refers to its partition into discrete, non-overlapping cells or elements. Each element is defined by a set of vertices and bounded by faces (Versteeg and Malalasekera, 2016). Consider the generic cell shown in Figure 4.1.

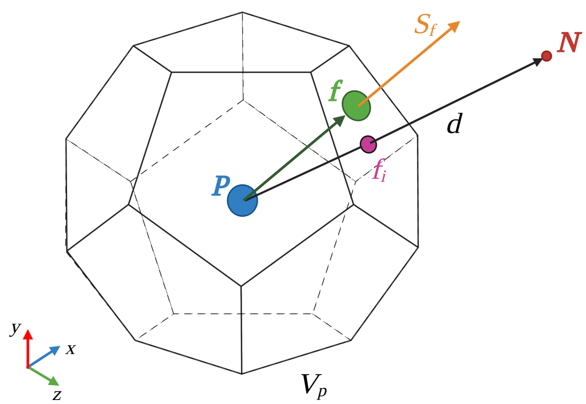

Figure 4.1. FVM cell in the solution domain.

According to the FVM, and in agreement with (Guerrero, 2019), one should know about each cell the following information: The control volume V_P has a volume V and has a centroid, which is point $\mathbf{P}$. Considering a contiguous cell with control volume V_N, the vector from the centroid $\mathbf{P}$ of V_P to the centroid $\mathbf{N}$ of V_N is named $\boldsymbol{d}$; the method also requires that all neighbors V_N of the control volume V_P are known. The control volume faces are labeled f, which also denotes the face center; The location where the vector $\boldsymbol{d}$ intersects a face is f_i. The face area vector V_f is at the face centroid, normal to the face, and has a magnitude equal to the area of the face; finally, the blue vector from the centroid $\mathbf{P}$ to the face center f is named P_f.

4.1.1 FVM DISCRETIZATION

The transport equation is a non-linear second-order equation. Its components include a temporal derivative, a convection term, a di usion one, and a source term. For good accuracy, the discretization order must be equal to or higher than the order of the equation. (Guerrero, 2019)

- Convection term.

  The discretization of the convection term brings to Equation 4.4

$$\int_{V_P} \nabla \cdot (\quad \mathbf{u}) dV \rightarrow \sum_f S_f \cdot (\quad \mathbf{u})_f \tag{4.4}$$

  Where su x f refers to the faces of a single control volume. Equation 4.4 needs the value of the parameter in the central point of the control volume, as well as the velocity and density values at each surface. This is controlled by theconvection di erencing scheme

- Di usion term.

  The discretization of the di usion term leads to Equation 4.5

$$\int_{V_P} \nabla \cdot (\ \nabla \ ) dV \rightarrow \sum_f S_f \cdot (\ {}_{\phi} \nabla \cdot \ )_f = S_c V_P \tag{4.5}$$

  In the case of having an orthogonal mesh, the di usion term is discretized by linearity. Non-orthogonality however, is usually more frequent, wherein it is common practice to split the term in two contributions, orthogonal and non-orthogonal, this must be considered when choosing the numerical schemes.

- Source term.

  The discretization of the source term renders as in Equation 4.6

$$\int_{V_P} S_{\phi} dV \rightarrow S_p V_P \ {}_P \tag{4.6}$$

  Source terms can be addressed as function of. And are linearized as well.

The fundamental properties of discretization schemes include conservativeness, boundedness, and transportiveness. Their breakdown and a comprehensive description of the many discretization schemes available are beyond the scope of this thesis. However, with this brief introduction to the FVM, the reader can further assess the following discussions.

4.1.2 DISCRETIZATION OF TWO-PHASE INCOMPRESSIBLE FLOW MODEL

The governing equations for the two-phase single uid incompressible model are re-written following the numerical discretization of the nite volime representation. The momentum equation results as:

$$\frac{@V\ \mathbf{u})_P}{@t} + \sum_f^N ((\ \ )_f \mathbf{u_f}) - \sum_f^N (\ \ _f \mathbf{S_f} \cdot (\nabla \mathbf{u_f})) = -\nabla p_d V_P - (\mathbf{g} \cdot \mathbf{x}) \nabla\ V_P + \nabla \mathbf{u} \cdot \nabla\ V_P$$

The discretized VOF convection equation considering the arti cial compression term is given by:

$$\frac{@V\ \ )_P}{@t} + \sum_f^N (\ \ )_f + \sum_f^N ((\ \ _r)_f\ \ _f (1 - \ \ _f)) = 0$$

Where the mass ux $(\ \ )_f$ is computed from the VOF ux $(\ \ )_f$ using the following relation:

$$(\ \ )_f = (\ \ )_f (\ \ _w - \ \ _a) + \ \ _f\ \ _a \tag{4.7}$$

Where, the subscript $_P$ describes averaged values of the owner cell, $_N$ the neighbour cells' averaged values, and $_f$ the averaged face values. Furthermore, $(\ _r)_f$ represents the relative velocity's ux, and the velocity face ux at the cell face f is given by:

$$_f = \mathbf{u_f} \cdot \mathbf{S_f} \tag{4.8}$$

(Kim, 2021), (Descamps, 2022), and (Choi, 2019) describe additional details on the discretization of the previous equations in the OpenFOAM context.

4.2 IMPLEMENTATION IN OPENFOAM & *FOAMSTAR*

The present work uses the open source C ++ library OpenFOAM-5 (OpenFOAM, 2023) in conjunction with the marine hydrodynamics library foamStar. This section discusses the characteristics of both libraries used for this thesis's numerical simulations.

OpenFOAM uses the second-order FVM with unstructured polyhedral meshes for general CFD applications. The library includes the two-phase solver interFoam (Deshpande et al., 2012), formulated for solving the VOF model and including the semi-implicit and second order in time MULES algorithm (Multi-dimensional Limiter for Explicit Solution), developed by co-founder and member of the OpenFOAM foundation, Henry Weller (Greenshields, 2020). The algorithm ensures the boundedness of the phase fraction field (strictly between 0 and 1).

foamStar is an in-house library co-developed by Bureau Veritas and Ecole Centrale de Nantes with special modules for wave generation and floating body dynamics (Monroy et al., 2016), with simmilar capabilities as interFoam, and waves2foam(Li et al., 2019).

4.2.1 SOLVER ALGORITHM

To solve the WSI problem the foamStar library uses a segregated algorithm. Therefore, instead of solving for all the unknowns and couplings at once, the segregated approach subdivides the problem into steps and they are solved sequentially. Usually, each step represents a single physics problem, but sometimes one step can involve multi-physics problems (COMSOL, 2023). foamStar's algorithm can be divided into three main steps, a time loop, a PIMPLE loop, and a PISO loop. This is, after the wave field has been initialized with the HOS' input wave. Figure 4.2 depicts a simplified version of the algorithm.

The PIMPLE algorithm is an hybrid formulation between the Semi-Implicit Method for Pressure-Linked Equations (SIMPLE), and the Pressure Implicit with Splitting of Operator (PISO). This method is formulated for very large time-steps and pseudo-transient simulations (Guerrero, 2019). The SIMPLE algorithm is a pressure-corrector method. As stated by (F. Moukalled, 2016), the solution is found iteratively by generating pressure and velocity fields that consecutively satisfy the momentum and continuity equations, while approaching the final solution (which satisfies both equations) at every iteration. In the PISO algorithm instead of solving all the coupled equations on an iterative fashion, the operators are split into an implicit predictor and, multiple explicit corrector steps. Therefore it is not considered as an iterative scheme, which explains one of the main differences with the SIMPLE algorithm:

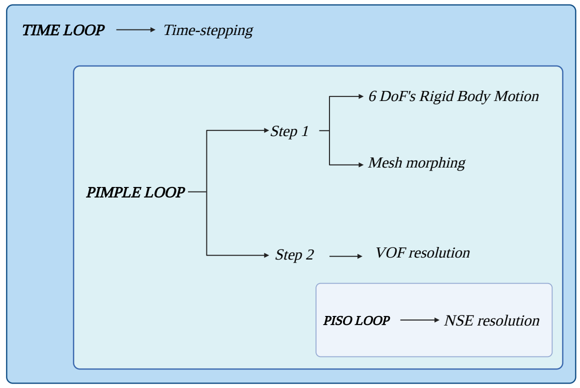

Figure 4.2. Simplified segregated algorithm steps for WSI solving in foamStar

not under-relaxation is applied and very few corrector steps are needed to obtain the desired accuracy. It is considered overall, an efficient method to solve the Navier-Stokes equations in unsteady problems.

The PIMPLE solution algorithm is updated by following the computational procedure:

- The dynamics of the body is solved by using a mechanical solver.
- The computational mesh of the viscous flow model is updated from the displacement of the body surface.
- The volume fraction transport equation is solved by MULES algorithm.
- is relaxed with the target values in the relaxation zone.
- NS or RANS equations are solved by PISO algorithm.
- The velocity is relaxed, but the pressure is not due to mass conservation.
- Check on the convergence parameters.

Figure 4.3 shows a simplified diagram of the entire computation algorithm. The algorithm's flow is the same as the interFoam solver, but extra stages are added in the foamStar library, shaded in light-purple on the Figure 4.3.

4.2.2 NUMERICAL ALGORITHMS

In OpenFOAM and foamStar the `system` dictionary contains the `fvSolution` file, which controls the options related to the pressure-velocity coupling method. The PIMPLE method works very similar to the PISO method. In fact, setting the keyword `nOuterCorrectors` to 1 is equivalent to running using the PISO method. To account for mesh non-orthogonality an

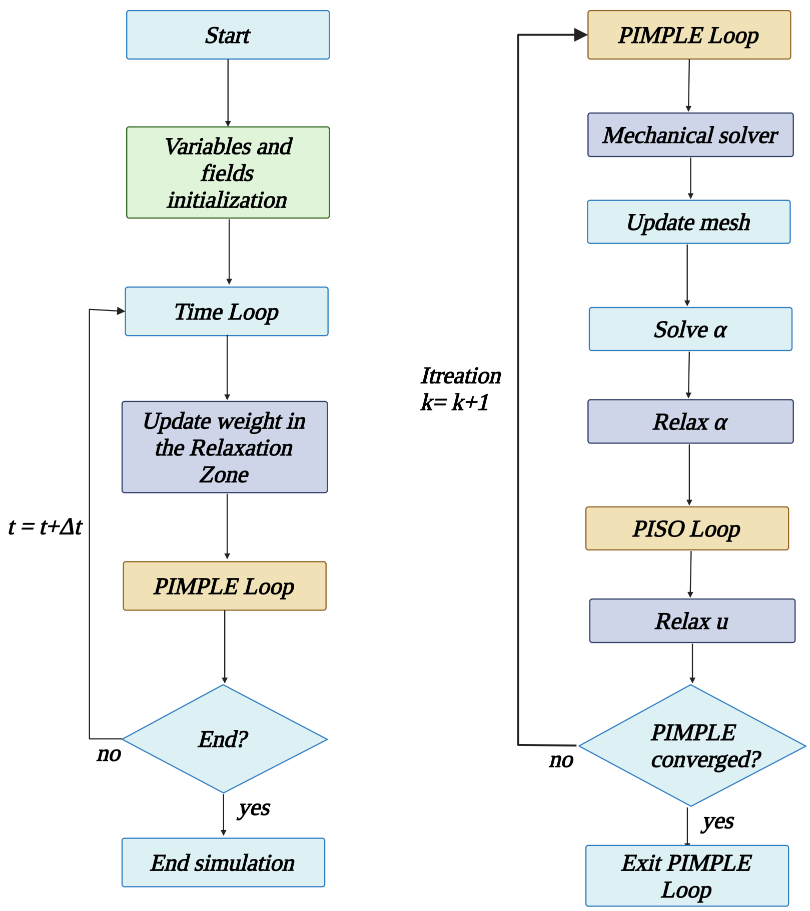

Figure 4.3. foamStar's simpli ed computation algorithm

additional corrector parameter is included, where the number of correctors is speci ed by the `nNonOrthogonalCorrectors` keyword. The number of non-orthogonal correctors is chosen according to the mesh quality. For orthogonal meshes one can use 0, whereas, for non-orthogonal meshes it is recommended to do at least 1 correction. Another sub-setting of `fvSolution` that is often used in OpenFOAM is `relaxationFactors`, which controls under-relaxation, a technique used for improving stability of a computation, particularly in solving steady-state problems. Under-relaxation works by limiting the amount which a variable changes from one iteration to the next, either by modifying the solution matrix and source prior to solving for a eld or by modifying the eld directly (Guerrero, 2019).

In OpenFOAM, the equation solvers, tolerances, and algorithms are controlled from the sub-setting control `solvers` located in the `fvSolution` dictionary le, the `solvers` settings specify each linear-solver that is used for each equation being solved; The syntax for each entry uses a keyword that is the word relating to the variable being solved in the particular equation and the options related to the linear-solver.

On this research, the `GAMG` method (geometric-algebraic multi-grid), was chosen for symmetric matrices (e.g., pressure) and the `cellDisplacement`. The generalized method of (GAMG) generates first a quick solution on a mesh with a small number of cells; maps this solution onto a finer mesh, using it as an initial guess to obtain an accurate solution on the fine mesh. `GAMG` is faster than standard methods when the increase in speed by solving first on coarser meshes outweighs the additional costs of mesh refinement and mapping of field data (Guerrero, 2019). The agglomeration of cells is performed by the algorithm specified by the `agglomerator` keyword. On the present thesis, the `faceAreaPair` method is used. Smoothing is specified by the `smoother`, the `DIC` smoother is the one used in this study.

The asymmetric matrices are assembled from the velocity ($\mathbf{u}$) and the transported quantities ( ), for them this thesis uses the `smoothSolver` method with `symGaussSeidel` smoother. The phase fraction uses the same configuration above described but with the additional MULES corrector terms. This type of solver is based on the Gauss-Seidel Method.

Table 4.1 shows the numerical algorithms used in this thesis, following OpenFOAM's and foamStar's notation.

Note: The solver tolerance should represent the level at which the residual is small enough that the solution can be deemed sufficiently accurate. The solver relative tolerance limits the relative improvement from initial to final solution, since the linear solvers will iterate until reaching any of the tolerance values set by the author.

4.2.3 NUMERICAL SCHEMES

The numerical schemes are defined in the `system` dictionary, inside the `fvSchemes` file. They have been chosen by following instructions and suggestions provided by previous authors, experienced on the the OpenFOAM's and foamStar implementation in the ocean engineering context (Descamps, 2022), (Kim, 2021). The schemes used on this thesis' simulations are collected in the Table 4.2.

The reader is encouraged to review the explanation in (Descamps, 2022) regarding the choice of time schemes to be used properly in conjunction with the MULES solver so that the boundedness of the phase fraction can be ensured. The Euler-type, crank-Nicholson with predictor, or backward MULES schemes have rendered accurate and stable results.

4.2.4 BOUNDARY CONDITIONS

In this thesis the following Dirichlet's boubdary conditions were used,

- `slip`: It is used as a slip constraint in the bottom of the NWT.
- `waveVelocity`: Imposes the velocity field at the boundary as equal to the target solution of the user-defined incident wave field.
- `pressureInletOutletVelocity`: This condition is applied to pressure boundaries where the pressure is specified. A zero-gradient condition is applied for outflow (as defined by the flux); for inflow, the velocity is obtained from the patch-face normal component of the internal-cell value (Greenshields, 2017).
- `movingWallVelocity`: This condition forces the velocity on the `wall` patches to be equal to the solved wall velocity from the rigid body motion.
- `waveAlpha`: Forces the volume fraction to adopt the user-defined value for the incident wave field.
- `inletOutlet`: This condition provides a generic outflow condition, with specified inflow for the case of return flow. In this thesis the value is set to zero, and it is used for the top boundary in the phase fraction dictionary.
- `totalPressure`: Since it is a constraint on the total pressure it is composed by an user defined value, plus a dynamic term. It is used for the top boundary.

The Neumann boundary conditions used are,

- `zeroGradient`: Applies a zero-gradient condition from the patch internal field (the center value of the owner cell) onto the patch faces. Therefore, the surface normal gradient is set to zero.
- `fixedFluxPressure`: Is imposed on the body boundary in this thesis, and forces a consistent surface normal gradient for the pressure field according to the system of governing equations.

Finally, the `symmetryPlane` boundary condition is used in this thesis since only half of the MPP is simulated. The condition suppresses the component of the vector field that is orthogonal to the symmetry plane. In foamStar, the initial and boundary conditions are defined within the `0` dictionary. Table presents the summary of the conditions specifying their field and respective boundary.

Matix system resolution		
Solved field	**Parameter**	**Reference values**
p_rgh	solver	GAMG
	smoother	DIC
	tolerance	1E-08
	relTol	0
U; k; omega	solver	smoothSolver
	smoother	symGaussSeidel
	tolerance	1E-07
	relTol	0
alpha	solver	smoothSolver
	smoother	symGaussSeidel
	tolerance	1E-08
	relTol	0
cellDisplacement	solver	GAMG
	tolerance	1E-07
	relTol	0
PIMPLE and PISO parameters		
Parameter		**Reference values**
momentumPredictor		yes
nOuterCorrectors		15
nCorrectors		3
nNonOrthogonalCorrectors		2
correctPhi		no
VOF resolution		
Parameter		**Reference values**
nAlphaCorr		2
cAlpha		0.6
alphaOuterCorrectors		yes
MULESCorr		yes
nLimiterIter		5
nAlphaSubCycles		1

Table 4.1. Numerical algorithms used for this thesis's simulations.

Numerical schemes		Reference values
Time schemes		
ddtScheme	default	Euler
		CranckNicolson 0.95
Cell-centered gradient schemes		
gradSchemes	default	cellLimited Gauss linear 1.0
Face interpolation schemes		
divSchemes	default	Gauss linear
	div(rhoPhi,U)	Gauss linearUpwindV GradU
	div(phi,alpha)	Gauss vanLeer
	div(phirb,alpha)	Gauss linear
	div(rhoPhi,k)	Gauss upwind
	div(rhoPhi,omega)	Gauss upwind
laplacianSchemes	default	Gauss linear corrected
interpolationSchemes	default	linear
Surface normal gradient schemes		
snGradSchemes	default	corrected

Table 4.2. Numerical schemes used for this thesis's simulations.

Field	Inlet; Outlet; Side	Bottom	Top	Body
U	waveVelocity	slip	pressureInletOutletVelocity	movingWallVelocity
alpha	waveAlpha	zeroGradient	inletOutlet	zeroGradient
p_rgh	zeroGradient	zeroGradient	totalPressure	xedFluxPressure

Table 4.3. Boundary conditions used for this thesis's simulations.

Part III

Ocean Engineering Application

Chapter 5

Blue Growth Farm

This chapter presents the speci c arrangements considered to marry the theory discussed in previous sections and the numerical simulations for the Blue Growth Farm (BGF) platform in the foamStar environment. The author presents the computation scenarios, and the numerical set-up for the BGF structure. The chapter aims to describe the procedures in a way that future researchers can reproduce and further extend the methodology for similar ocean engineering problems.

5.1 BODY DEFINITION

The experimental campaign for the BGF structure was conducted at École Centrale de Nantes, according to specifications from the project consortium (Ohana et al., 2023). A 1:40th scaled model of the BGF was built in aluminum. Table 5.1 presents the model's relevant information.

Parameter	**1:1**	**1:40**	**Units**
External size	210x162	5.25x4.05	m
Moonpol size	172x124	4.30x3.10	m
Draft	20	0:49	m
Mass	2:13e8	3384	kg
Moment of inertia I_{xx}	7:28e8	7100	kgm^2
Moment of inertia I_{yy}	1:09e9	10600	kgm^2
Moment of inertia I_{zz}	1:80e9	17600	kgm^2

Table 5.1. Blue Growth Farm structure information.

The mass and inertia properties of the structure are defined in the foamStar environment inside the `dynamicMeshDict` file, located in the `constant` folder. The name of the file reveals its function, it is where the user sets all body motion and mesh morphing parameters. The mass and inertia values read as,

```
mass                        3384;
momentOfInertia        (7109.375 10644.53125 17578.125  0 0 0);
```

The inertia values were calculated following scaling rules described in (Ruzzo et al., 2021). The first three components in the `momentOfInertia` entry must correspond to the diagonal values of the 9-component Inertia matrix, since, it corresponds to the way the later is defined in foamStar. The definition allows the user to input all the components of the matrix, if relevant. And, in case the user does not define the `momentOfInertia` value, the software considers the identity matrix as default.

Another important parameter to define for the body motions is the `CorInitial`. This thesis considers the fixed body reference frame at the body's center of gravity. It is also assumed that the position of the center of gravity and center of rotation are the same. By setting the aforementioned parameter, the motions and forces are calculated respect to this point. Figure 5.1 depicts the coordinate systems considered for the simulations. The reader is encouraged to refer to (Descamps, 2022) and (Kim, 2021) for additional details on the rigid body motions and mesh morphing procedures in foamStar.

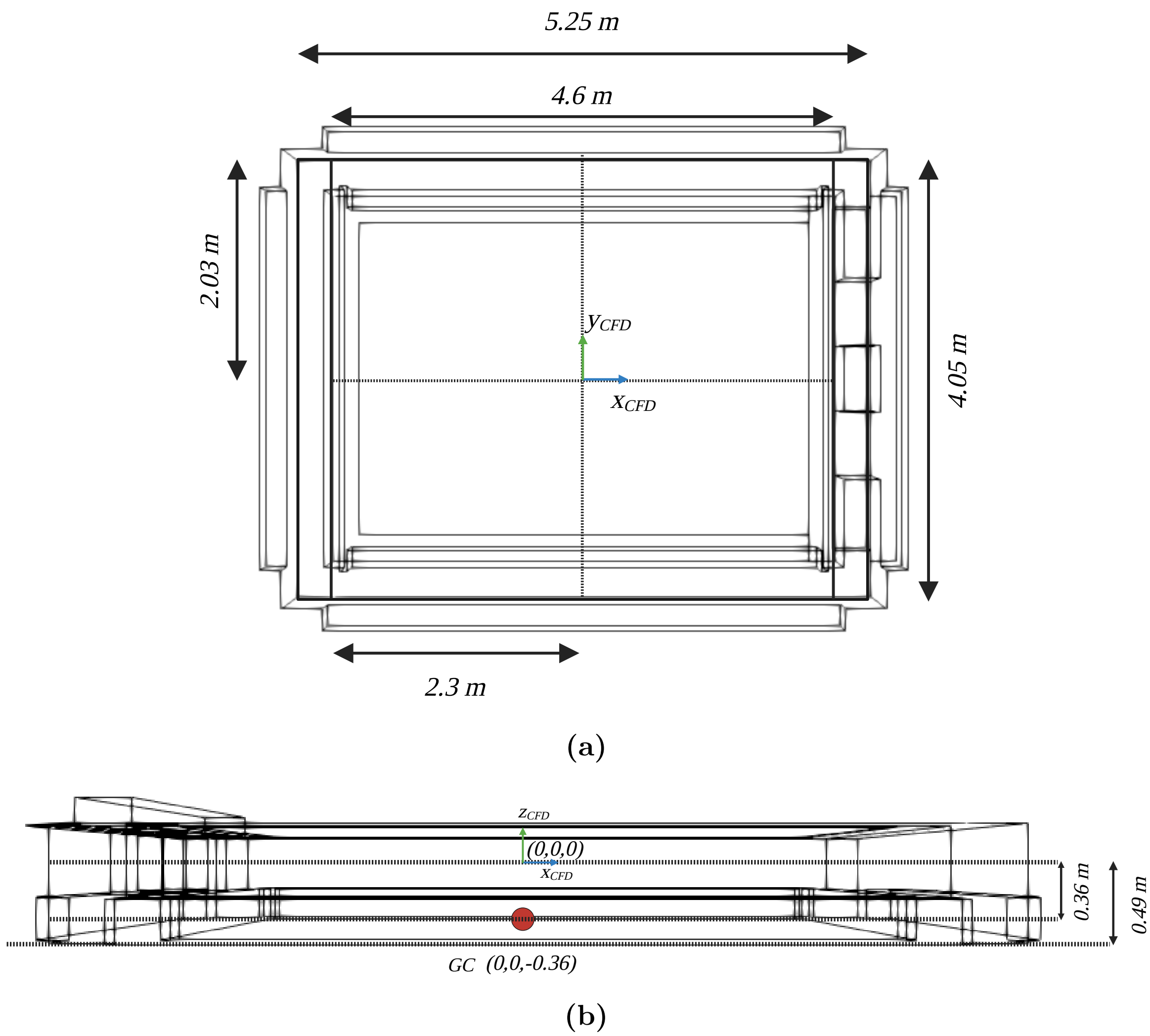

Figure 5.1. Model dimensions.(a) Top view. (b) Side view, Center of Gravity and rotation.

In this thesis the author takes advantage of the structure's symmetry when defining the numerical domain. The CFD geometry accounts for half of the model's dimension. At this point the `symmetryPlane` boundary condition is imposed so that results are consistent with the full geometry counterpart, with a gain in computational time.

5.2 COMPUTATIONAL DOMAIN AND MESHING TECHNIQUE

The adopted meshing process initially defines a domain which encloses the geometry for an hexahedral and typically uniform mesh, this is achieved by means of the blockMesh dictionary and command. The enclosing domain—the CFD domain— is defined as a function of the wavelength L, also found in literature as . Figure 5.2 depicts the configuration used in this thesis. Normally, below the free-surface level, the bottom boundary could be located one below; this study considers a depth of five meters to try and reproduce the experimental dimensions as closely as possible.

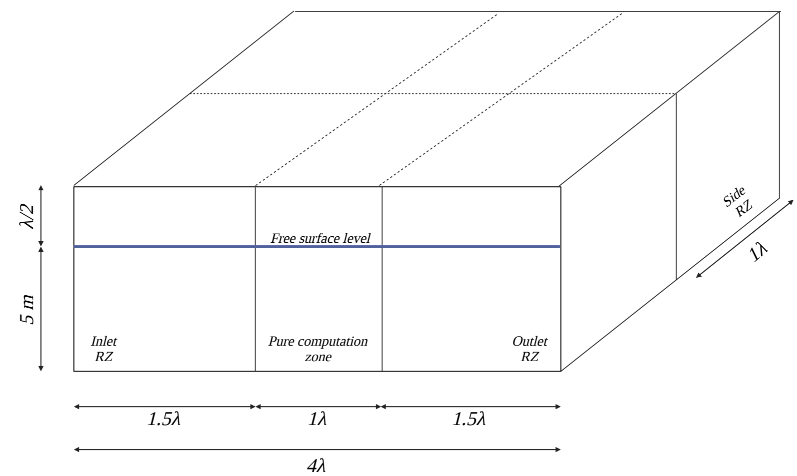

Figure 5.2. Computational domain definition as function of wavelength .

However, in this study the author defines non-uniform meshes that relate cell dimensions x and z with the wave height H and wavelength L or , in the free-surface zone. This mesh configurations are motivated by the experience collected by previous researchers (Kim, 2021), (Descamps, 2022), where their discoveries indicate that, to ensure a proper wave propagation, one should ensure at least 100 cells per, and 12 cells per H in the free-surface zone. As a result, cells in the free-surface zone are not always isometric, whereas cells in the other zones are. Figure 5.3 illustrates the non-uniform meshes for the regular and irregular wave propagation studies, and their refinement zones.

The mesh development starts with the blockMesh considering the number of cells for the coarser zones. After this base-mesh, one can specify the blocks for refinement using the `topoSet` dictionary. And each refinement is carried out with the `refineMesh` command, which refines each cell by a factor of 1=2. Once the base-mesh is achieved, the `surfaceFeatures`

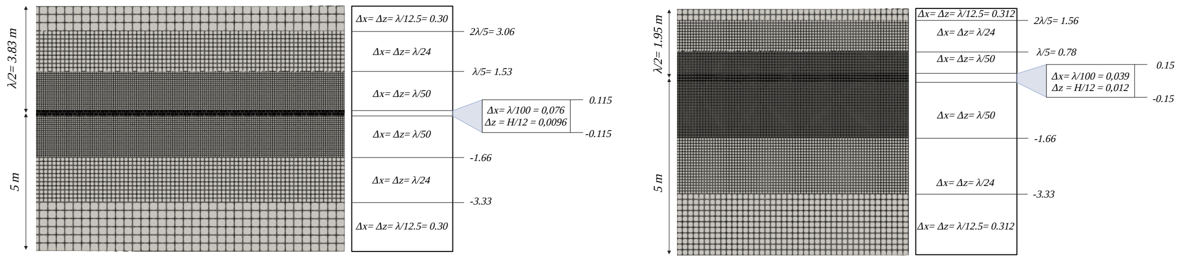

(a) (b)

Figure 5.3. Non-uniform mesh for wave propagation.(a) Regular wave. (b) Irregular wave.

command reads the .STL geometry in the`constant/triSurface` folder, extracts the edges from it and writes them in a .eMesh le that latter is used in the `snappyHexMeshDict` le. The nal mesh is generated by snappyHexMesh, an utility that is part of the OpenFOAM package. snappyHexMesh generates three dimensional meshes containing hexahedra (hex) and split-hexahedra (split-hex) elements generated automatically from triangulated surface geometry in the stereolithography (STL) format. The mesh gradually conforms to the surface by iteratively re ning a starting mesh and morphing the resulting split-hex mesh to the surface. An optional phase will shrink back the resulting mesh and insert cell layers. The speci cation of mesh re nement level is very exible and the surface handling is robust with a pre-speci ed nal mesh quality. Figure depicts the three-dimensional meshes obtained for the regular and irregular wave-cases considered in this study.

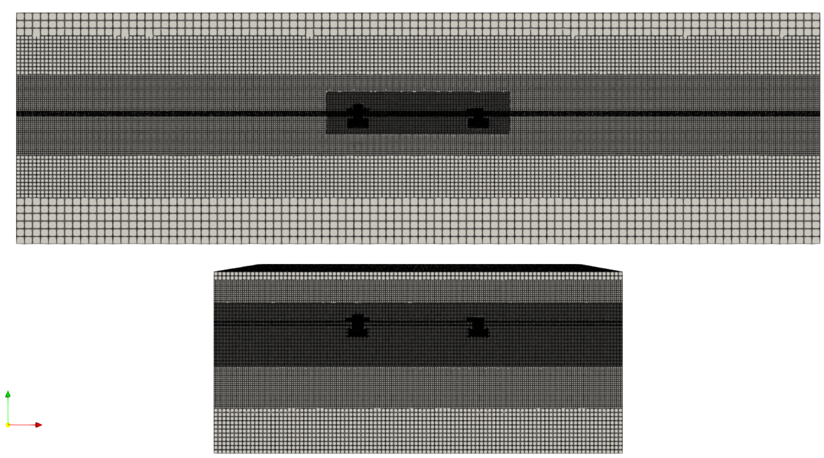

Figure 5.4. Three-dimentional meshes generated withsnappyHexMeshutility. Top for regular wave, bottom for irregular wave.Â

5.3 INCIDENT WAVES

This thesis aims to simulate two wave-scenarios. One regular and one irregular wave set-up have been developed in the foamStar context. Table 5.2 summarizes the important parameters for each. These are set in the `waveProperties` or `waveTrains` les for the numerical simulation.

Regular waves		Irregular waves		Units
H	0.115	Hp	0.15	m
P	2.21	Tp	1.58	s
lambda	7.66	lambda	3.89	m
		Gamma	3.3	-

Table 5.2. Wave parameters.

These les must contain not only the information consigned in the Table, they also specify the wave model to use and its parameters. Since this thesis uses the HOS model, the `Grid2Grid` dictionary must be also inside the `constant` folder, to be able to link the HOS mesh and incident wave information with the foamStar environment. Furthermore, this thesis implements the Relaxation Zones techniques, described in previous chapters. With all this considerations, Figure illustrates the nal set-up used in this study for the wave generation and absorption. For illustration purpose the gure re ects the regular case set-up, but it is of course applicable to the irregular case as well.

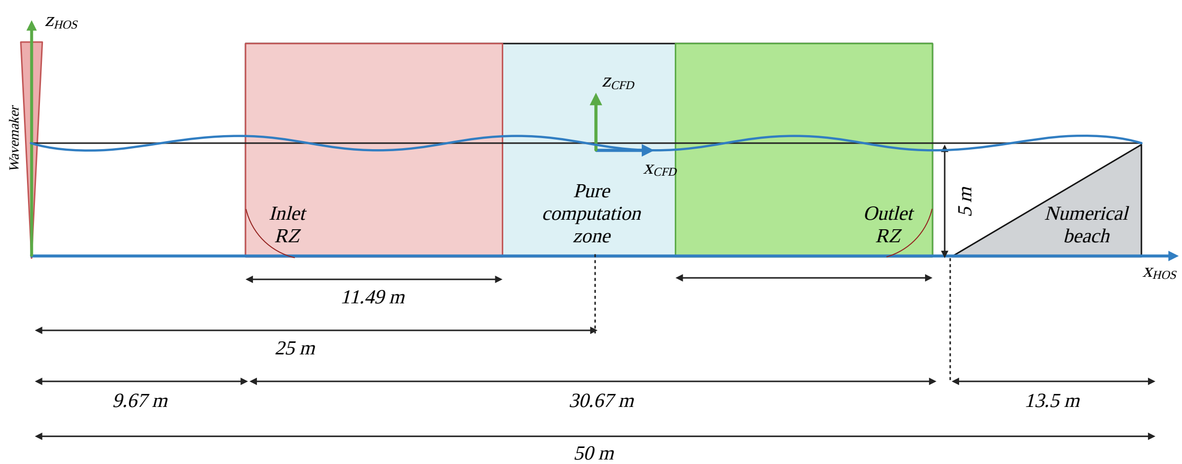

Figure 5.5. Wave generation model: HOS-RZ.

5.4 MOORING ARRANGEMENT

The mooring arrangement considered in this thesis is a scaled version of the experimental set-up. The scaling of the `fairleadDistance` and `anchorDistance` parameters is in function of the numerical domain considered. This parameters are set in the `dynamicMeshDict` file, located in the `constant` folder. This thesis assumes the mooring arrangement as a spring-like system. Figure 5.6 depicts both the experimental and numerical arrangements.

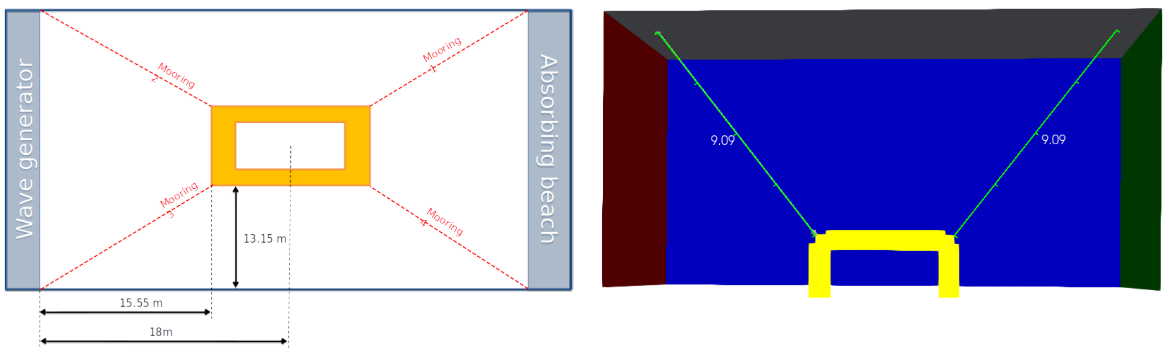

Figure 5.6. Mooring arrangement.

Chapter 6

Results and discussion

This section collects the results obtained using thefoamStar solver to simulate the BGF case. The results that are more relevant to this study are those regarding body motions and free-surface elevation.

6.1 QUASI-STATIC CASE

The quasi-static simulations are useful when analyzing the behavior of the structure and solver when there is no action from incoming waves. In this sense, it is possible to determine important parameters before moving on to more complex simulations. One can check parameters such as temporal and spatial discretization when obtaining the quasi-static results since it is possible to expect a certain type of behavior for the body motions, especially with the experimental results. In that sense, the quasi-static simulations are practical and less time-consuming. This is the first step to hierarchically developing more robust simulations.

Two quasi-static simulations were performed, being different in domain definition and spatial discretization. The coarser meshes were generated with the StarCCM+ package as part of the initial attempt to simulate the BGF case back in 2021. The second mesh was generated via blockMesh and snappyHexMesh, as reported in previous sections. Figure 6.1 depicts both meshes.

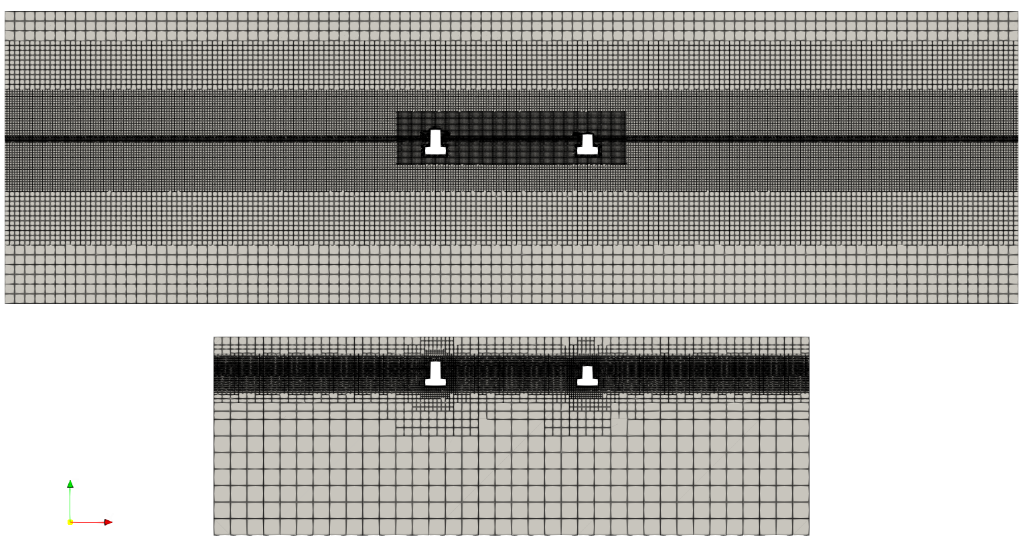

Figure 6.1. Mesh used for the quasi-static simulations.

Figure 6.2 illustrates the results. It is evident that the numerical domain and spatial discretization used in the first attempt do not make the platform's motions coherent with the expected behavior. From these very first simulations, the author is able to confirm the importance of the mesh discretization suggested by previous authors (Descamps, 2022), not only for the wave propagation but also for the body motions, since the mesh and mesh-morphing appear to signi cantly in uence the results of the simulations. Table 6.1 reports details of each mesh.

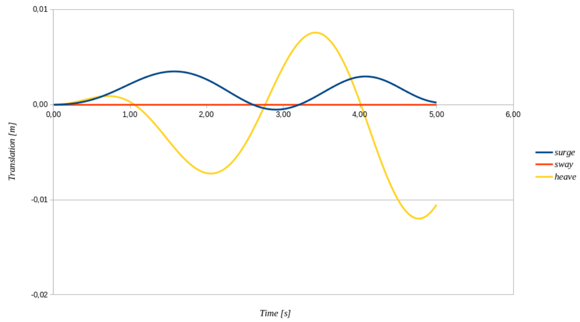

(a)

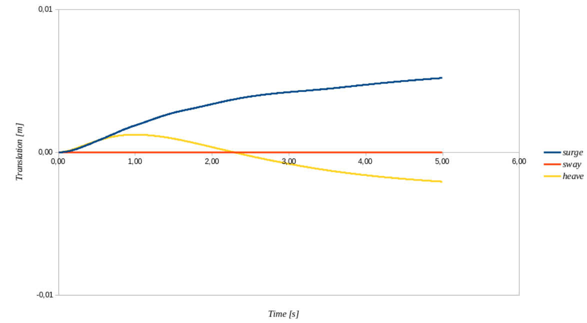

(b)

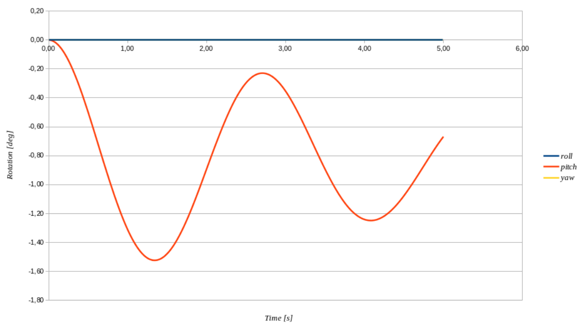

(c)

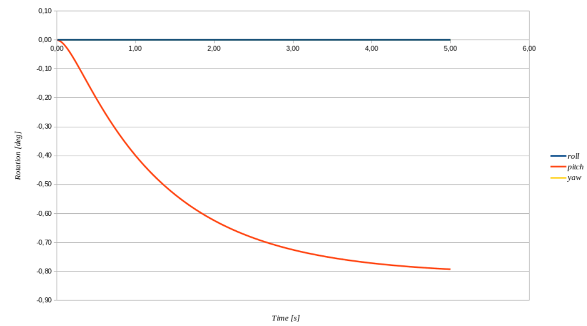

(d)

Figure 6.2. BGF's motions under quasi-static simulations. (a) & (b) Translation using medium and coarse mesh, respectively(a) & (b) Rotation using medium and coarse mesh, respectively.

	Coarse	Medium
Mesh stats		
points	2311531	7749901
faces	6110718	22035381
internal faces	5644713	21458628
cells	1892250	7143243
faces per cell	6.2124	6.088
boundary patches	7	7
point zones	0	0
face zones	0	0
cell zones	0	0
Checking geometry		
Max aspect ratio	25.8911	12.316
Minimum face area	3.20235039305e-07	6.79930205484e-07
Maximum face area	0.25	0.102221449723
Min volume	4.23878037917e-09	8.19756347665e-08
Max volume	0.125	0.0300993848941
Total volume	645.981825853	2706.53294641
Mesh non-orthogonality Max	79.9750121379	77.7436739843
average	10.0473	5.253
Face pyramids	OK	OK
Max skewness	4.8411	2.6161

Table 6.1. Mesh' statistics.

6.2 WAVE PROPAGATION IN NWT

One of the aspects that received more attention from the author in this thesis was the proper generation of incident waves that would be as close as possible to the waves generated at the ocean's basin used for the experimental campaign. In this sense, this is the reason why the HOS pseudo-spectral model was used instead of the stream function model typically used for regular waves. As explained in previous sections, the HOS methodology developed at LHEEA enables the use of a ramp time that is in accordance with the experimental set-up.

The methodology adopted to validate the waves consisted rst of comparing the HOS output with the experimental values. Once the output from HOS was veri ed to give coherent results, the author moved on to numerical simulations coupling the incident HOS waves and foamStar's wave models. The free-surface elevation experimental measurements obtained at speci c wave gauges were compared with their numerical counterparts after the due scaling process to place them consistently inside the computational CFD domain. The arrangement of wave-gauges used for the experiments is depicted in Figure 6.3. The distances are scaled in this thesis as a function of the computational domain under consideration.

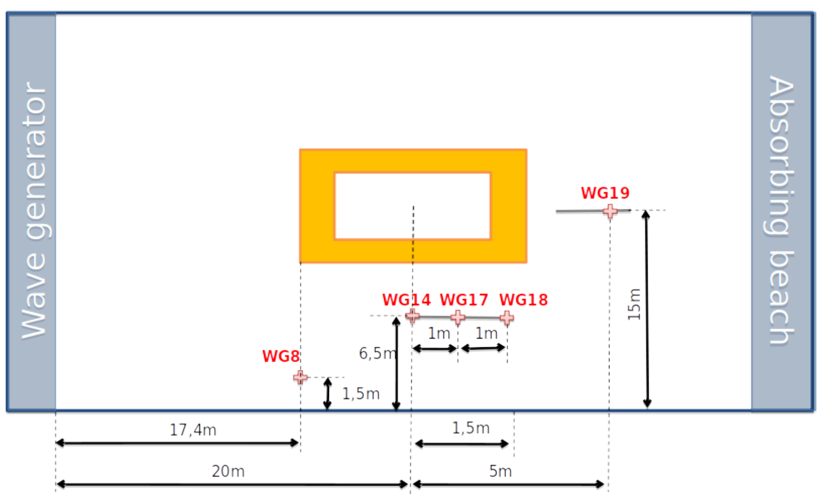

Figure 6.3. Wave gauges' arrangement on the experimental campaign.

The wave-propagation study was performed considering 2-Dimensional meshes, generated from the 3-Dimensional `blockMesh` base-mesh with the `extrudeMesh` command. Figure 6.4 shows the results.

It is relevant to notice that the numerical probes inside the foamStar library are yet to be revised. The results obtained with them are not consistent with the physics of the problem.

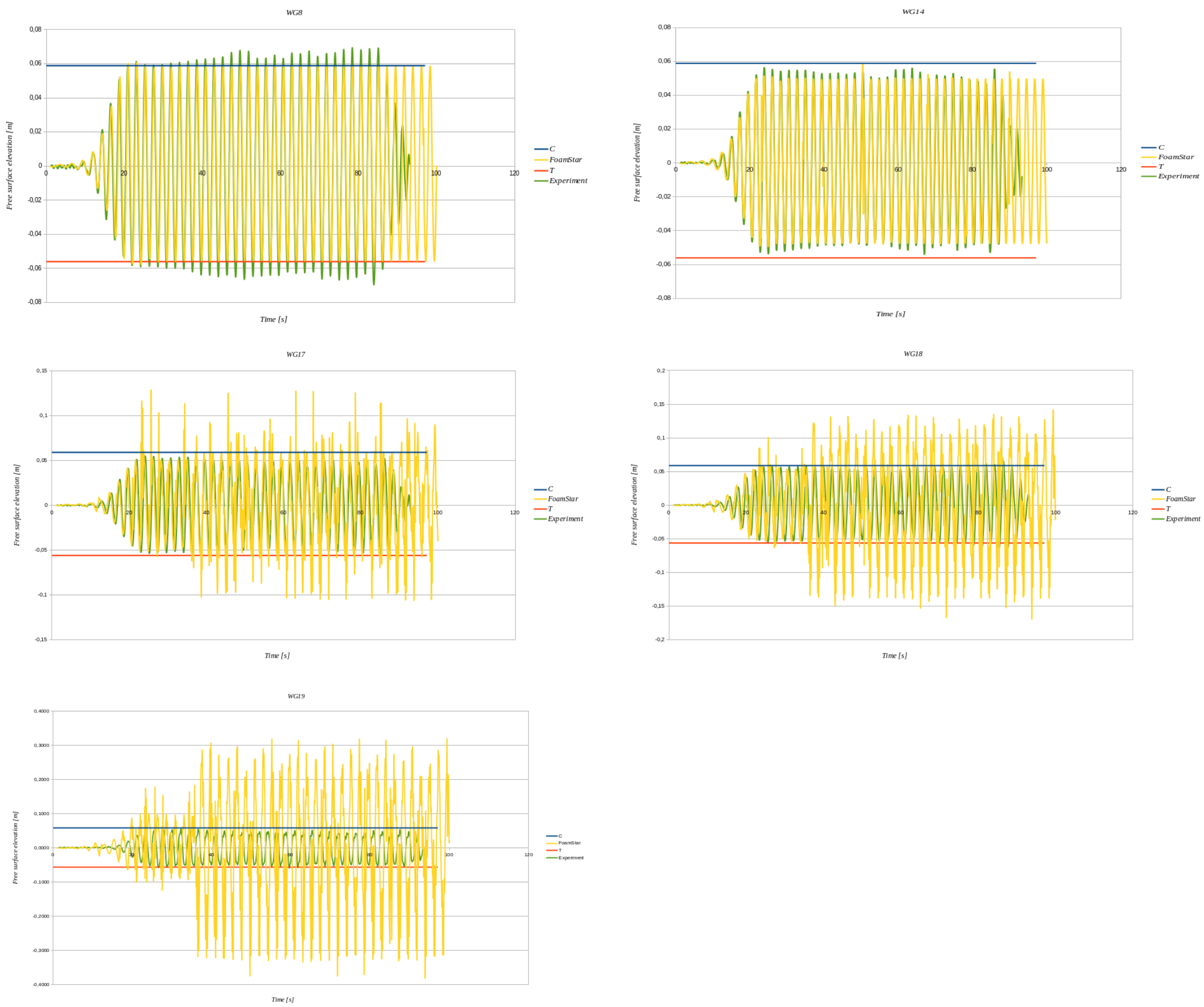

Figure 6.4. Comparison of free-surface elevation values between 2-Dimensional wave simulations and experimental results.

Therefore, the plots presented here used a C++ code developed by the author of (Descamps, 2022). The code takes as input the free-surface .vtk's obtained from the simulation and a .txt le containing the coordinates of the points of interest. The output is the free-surface values at such points through the entire simulation. The code was not developed in an industrial or very rigorous concrete manner, but rather to cope with the lack of functioning of the foamStar's probes. That is one of the reasons for the spikes appearing on the plots. The rst two gures —for WG8 and WG14— were manually cleaned so that the reader could better appreciate the coherence between the experimental and simulated data, even under the assumption of a 2-dimensional computational domain.

However, the \spiky" behavior also increases as the wave probe goes farther from the wave-maker. At this moment, it is not clear if there are reasons beyond the probes for this behavior, and it needs to be investigated further, considering di erent ways of acquiring the free-surface elevation data. Nonetheless, the results are promising and constitute another major difference from the rst BGF's simulation attempt, where the considered waves followed the stream-function theory without the initial ramp. Figure 6.5 illustrates the history of the residual values through the wave-propagation simulation. From the plot, it is possible to note a non-monotonic convergence.

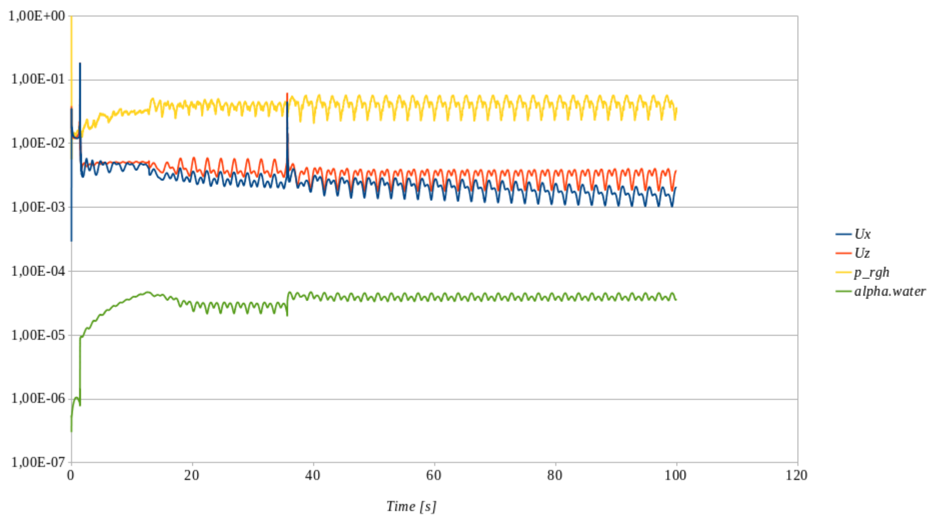

Figure 6.5. Residuals' history for two-dimensional wave propagation simulations.

6.3 REGULAR WAVES

The next step in the hierarchical approach adopted for this problem is to try and simulate the wave-structure interaction problem for the BGF case after having considered the spatial discretization and the proper wave propagation. The case takes signi cant time since it involves the solution of body motions, wave propagation, the uid's variables, mesh morphing procedures, and the inclusion of the mooring arrangement, all interacting at each evaluation of the numerical algorithms discussed in previous sections. Results from the numerical simulation are depicted in Figure 6.6. Evidently, after approximately 32 seconds of physical time the simulation crashed and values for surge and roll sky-rocketed.

Furthermore, Figure 6.7 overlaps the results from the numerical simulation with those obtained from the experimental campaign. The results not only do not agree with the experimental

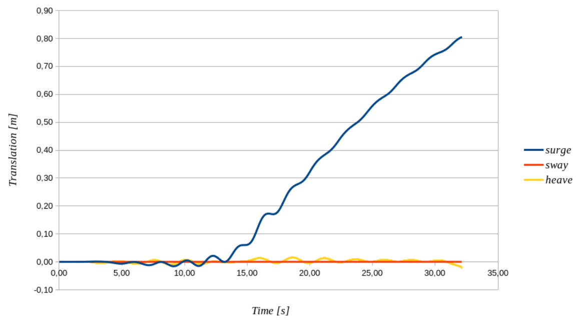

(a)

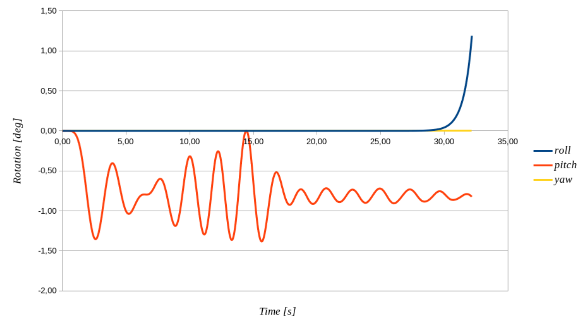

(b)

Figure 6.6. BGF's motions from foamStar's 3-D Regular wave and structure interaction simulations. (a) Translation. (b) Rotation.

values, but they also don't agree much when analyzing the possible movements that the platform could undergo. Some variables show divergent behavior, while others seem to maintain a trend. At this time, it is uncertain if the time discretization could have such e ects since no sensitivity study has been conducted in this regard. However, the author could be more inclined to believe that the mooring arrangement should be checked in more detail; this could be a signi cant source of discrepancy, especially for the motion variables.

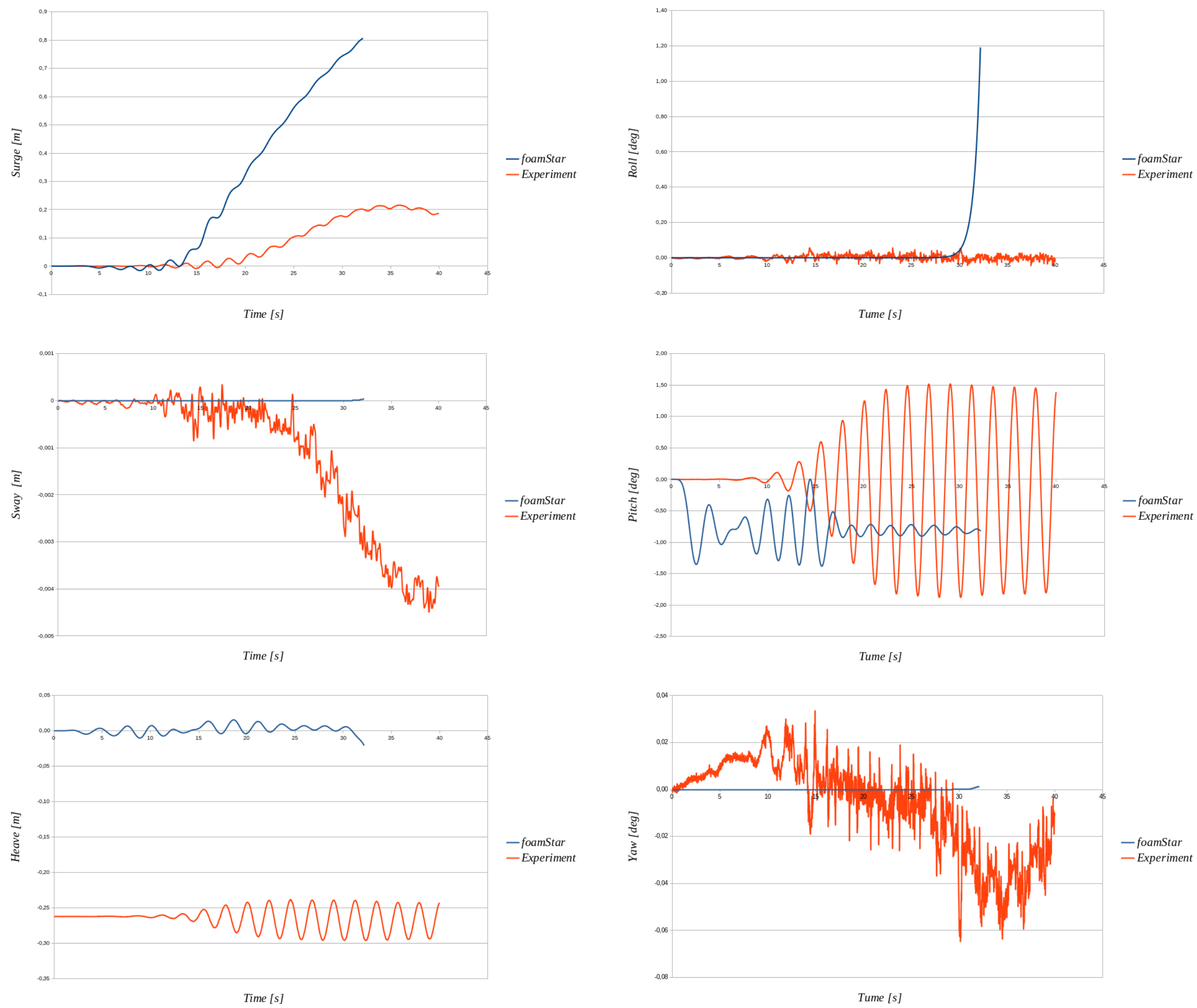

Figure 6.7. Comparison of BGF's motion values betweenfoamStar's 3-D Regular wave-structure interaction simulations and experimental results.

6.4 IRREGULAR WAVES

At the time of this thesis submission, the irregular wave case is still running. The computational domain and 3D mesh were generated successfully. As well as the incident wave eld using the HOS-NWT solver, fully coupled simulations are currently running on the GLiCID cluster, which was put into service only at the beginning of August. Further developments and results are expected in the upcoming days.

Part IV

Epilogue

Chapter 7

Epilogue

7.1 CONCLUSIONS

This thesis proposes a framework for the analysis of some of the responses generated by the BGF platform when subjected to regular and irregular wave action. To do so, this thesis included the synthesis of theoretical knowledge and the implementation of the nite volume methodology for a uid-structure interaction problem. Furthermore, the thesis incorporated a background on previous studies conducted to assess the design and development of multipurpose structures, rea rming the importance of continuing e orts to nd cleaner and smarter alternatives to the growing food and energy demand.

Three types of numerical simulations were conceived and described in this thesis. Two of them, with what the author believes to be encouraging results, are another step forward into unraveling this particular case. The results, even if few, show advancements with respect to the previous attempt to tackle the problem back in 2021. As mentioned at the beginning of this document, the ow of simulations was a ected by a change in the university's cluster. Nonetheless, the ndings solve some issues, but more importantly, they leave more questions. And what gives more meaning to the life of an engineer than the never-ending curiosity and eagerness to search for answers and solutions?

The author's two-year master's program culminated in the writing of this thesis, which tells a tale and compiles the information she gained. The theoretical chapters make an e ort to compile and condense the most important ideas discovered in the area of ocean and naval engineering. The writing style of this thesis, especially the portions that deal with the application and usage of thefoamStar solver, is what the author thinks makes the most contribution to the eld. The goal of this e ort is to help future researchers when they begin working with numerical simulations using software that they may not be acquainted with and that occasionally lacks documentation because of its continuous development. This work might serve as a reference for anybody who is interested in diving into the numerical simulations universe, from very basic yet essential concepts.

As a nal remark to the conscious reader: it becomes evident that simulating in open-source software has many advantages but also requires patient and stubborn users willing to read every forum and copy every tutorial in order to make their case work. On that note, for your patience, I thank you.

7.2 PERSPECTIVES AND FUTURE WORK

Individual component analysis, while necessary, is insufficient when several components are integrated into a single multi-purpose structure where their interaction is critical. As a result, several research methodologies must be implemented to enable proper observation of the coupling effects between the subsystems. Next attempts must focus on the proper mooring arrangement definition, since this thesis simplified the arrangement by modeling a spring-like system. The results from the irregular wave action must be analyzed and contrasted in order to determine more realistic effects that the platform could undergo in the marine environment. Furthermore, the inclusion of viscosity effects could be considered for future studies, particularly if other experimental conditions are to be reproduced. Finally, the synergy between the numerical robustness of the foamStar library and data acquisition and post-processing routines will be of enormous benefit for future researchers.

References

Abhinav, K., Collu, M., Benjamins, S., Cai, H., Hughes, A., Jiang, B., Jude, S., Leithead, W., Lin, C., Liu, H., Recalde-Camacho, L., Serpetti, N., Sun, K., Wilson, B., Yue, H., and Zhou, B.-Z. (2020). O shore multi-purpose platforms for a blue growth: A technological, environmental and socio-economic review. Science of The Total Environment, 734:138256.

Auer, M. S. G. Marine renewable integrated application platform. Electronically.

Boccotti, P. (2002). Caisson for absorbing wave energy.

Boccotti, P. (2015). Chapter 1 - wave mechanics: Basic concepts. In Boccotti, P., editor, Wave Mechanics and Wave Loads on Marine Structures, pages 1{23. Butterworth-Heinemann, Oxford.

Brito, J. H. (2015). Modular multi-use deep water o shore platform harnessing and servicing mediterranean, subtropical and tropical marine and maritime resources. Electronically.

Buresti, G. (2015). A note on stokes' hypothesis. Acta Mechanica, 226(10):3555{3559.

Choi, Y. (2019). Two-way Coupling between Potential and Viscous Flows for a Marine Application. PhD thesis.

Choi, Y., Gouin, M., Ducrozet, G., Bouscasse, B., and Ferrant, P. (2017). Grid2grid : Hos wrapper program for cfd solvers.

Comission, E. (2017). Final report summary: H2ocean (development of a wind-wave power open-sea platform equipped for hydrogen generation with support for multiple users ofenergy).

COMSOL (2023). Understanding the fully coupled vs. segregated approach and direct vs. iterative linear solvers.

Dalrymple, R. G. D. R. A. (1991). Water Wave Mechanics for Engineers and Scientists, volume 2 of Advanced Series on Ocean Engineering. World Scienti c Publishing Co. Pte. Ltd.

Descamps, T. (2022). Numerical analysis and development of accurate models in a CFD solver dedicated to naval applications with waves. PhD thesis, Ecole Centrale de Nantes.

Deshpande, S., Anumolu, L., and Trujillo, M. (2012). Evaluating the performance of the two-phase ow solver interfoam. Computational Science & Discovery, 5.

Dommermuth, D. and Yue, D. K. (1987). A high-order spectral method for the study of nonlinear gravity waves. Journal of Fluid Mechanics, 184:267 { 288.

Donea, J., Huerta, A., Ponthot, J.-P., and Rodriguez-Ferran, A. (2004). Arbitrary lagrangian-eulerian methods. volume 1, pages 413{437.

Ducrozet, G. (2007). Modelisation des processus non-lineaires de generation et de propagation detats de mer par une approche spectrale. PhD thesis.

Ducrozet, G., Bonnefoy, F., Le Touze, D., and Ferrant, P. (2007). 3d hos simulations of extreme waves in open seas. Natural Hazards and Earth System Sciences, 7(1):109{122.

Ducrozet, G., Bonnefoy, F., Le TouzÃ©, D., and Ferrant, P. (2012). A modi ed high-order spectral method for wavemaker modeling in a numerical wave tank. European Journal of Mechanics - B/Fluids, 34:19{34.

Ducrozet, G., Bonnefoy, F., Le TouzÃ©, D., and Ferrant, P. (2016). Hos-ocean: Open-source solver for nonlinear waves in open ocean based on high-order spectral method. Computer Physics Communications, 203:245{254.

European comission, D. G. f. M. A. and Fisheries (2012). Blue Growth Opportunities for marine and maritime sustainable growth. Luxembourg: Publications O ce of the European Union.

F. Moukalled, L. Mangani, M. D. (2016). The Finite Volume Method in Computational Fluid Dynamics: An Advanced Introduction with OpenFOAM and Matlab. Springer Cham, 1 edition.

Felippa, C., Park, K. C., and Farhat, C. (2001). Partitioned analysis of coupled system. Computer Methods in Applied Mechanics and Engineering, 190:3247{3270.

GLiCID (2023). Le groupement ligerien pour le calcul intensif distribue.

Greenshields, C. (2020). Interface capturing in openfoam.

Greenshields, C. J. (2017). Openfoam user guide version 5.0.

Guerrero, J. (2019). Crash introduction to the fvm and numerical playground. CC BY-SA license.

Hirt, C. and Nichols, B. (1981). Volume of uid (vof) method for the dynamics of free boundaries. Journal of Computational Physics, 39(1):201{225.

Jacobsen, N., Fuhrman, D., and Fredsoe, J. (2012). A wave generation toolbox for the open-source cfd library: Openfoam (r). International Journal for Numerical Methods in Fluids, 70.

Jeremy, O., Boris, H., Arnaud, M., Vincent, A., Bonnefoy Felicien, G., Brizzi, B., and Benjamin (2022). Wave tank testing of a multi-purpose platform with aquaculture, wind turbine and wave energy converters.

Kim, Y. (2021). Numerical improvement and validation of a naval hydrodynamics CFD solver in view of performing fast and accurate simulation of complex ship wave interaction. PhD thesis.

LHEEA (2023).

Li, L., Ruzzo, C., Collu, M., Gao, Y., Failla, G., and Arena, F. (2020). Analysis of the coupled dynamic response of an o shore oating multi-purpose platform for the blue economy. Ocean

Engineering, 217:107943.

Li, Z., Bouscasse, B., Ducrozet, G., Gentaz, L., Le TouzÃ©, D., and Ferrant, P. (2021). Spectral wave explicit navier stokes equations for wave structure interactions using two phase computational uid dynamics solvers. Ocean Engineering 221:108513.

Li, Z., Deng, G., Queutey, P., Bouscasse, B., Ducrozet, G., Gentaz, L., Le TouzÃ©, D., and Ferrant, P. (2019). Comparison of wave modeling methods in cfd solvers for ocean engineering applications. Ocean Engineering 188:106237.

Massel, S. R. (2017). *Ocean Surface Waves*, volume 45 of *Advanced Series on Ocean Engineering*. World Scienti c Publishing Co. Pte. Ltd., 3 edition.

Mayer, S., Garapon, A., and Sorensen, L. S. (1998). A fractional step method for unsteady free surface ow with applications to non linear wave dynamics. *International Journal for Numerical Methods in Fluids*, 28(2):293{315.

Monroy, C., Seng, S., and Malenica, S. (2016). Developpements et validation de l'outil cfd openfoam pour le calcul de tenue a la mer.

Ohana, J., Horel, B., Merrien, A., Arnal, V., Bonnefoy, F., Brizzi, G., Bouscasse, B., and Ruzzo, C. (2023). Wave tank testing of a multi-purpose oating platform with aquaculture, wind turbine and wave energy converters.

Ono, R. (2016). Human history of maritime exploitation and adaptation process to coastal and marine environments. a view from the case of wallacea and the paci c. In Marghany, M., editor, *Applied Studies of Coastal and Marine Environments*, chapter 16. IntechOpen, Rijeka.

OpenFOAM (2023).

Papandroulakis, N., Thomsen, C., Mintenbeck, K., Mayorga, P., and Hernandez-Brito, J. J. (2017). The EU-Project \TROPOS " , pages 355{374. Springer International Publishing, Cham.

Perez, Cristian Herran Cabrera & Andersen, D. B. . H. I. T. . L.-L. P. (2014). *Viability Strategy for the Deployment and Exploitation of Multiuse Marine Platforms: Modular multiuse deep water o shore platform harnessing and servicing Mediterranean, subtropical and tropical marine and maritime resources*. DTU Management Engineering.

Pirlet, H.; Claus, S. C. E. D. C. E. G. R. M. F. R.-K. S. J.-J. Z. B. . (2014). The mermaid project. innovative multi-purpose o shore platforms. Online, Flanders Marine Institute (VLIZ): Ostend.

Richter, T. (2010). Numerical methods for uid-structure interaction problems.

Richter, T. (2017). *Fluid-structure Interactions: Models, Analysis and Finite Elements*. Lecture Notes in Computational Science and Engineering. Springer Cham, 1 edition.

Rienecker, M. M. and Fenton, J. D. (1981). A fourier approximation method for steady water waves. *Journal of Fluid Mechanics*, 104:119{137.

Rusche, H. (2002). *Computational Fluid Dynamics of Dispersed Two-Phase Flows at High Phase Fractions*. PhD thesis.

Ruzzo, C., Muggiasca, S., Malara, G., Taru , F., Belloli, M., Collu, M., Li, L., Brizzi, G., and Arena, F. (2021). Scaling strategies for multi-purpose oating structures physical modeling: state of art and new perspectives.Applied Ocean Research108:102487.

Ruzzo, C., Romolo, A., Malara, G., Arena, F., Taru , F., Muggiasca, S., Belloli, M., Bouscasse, B., Ohana, J., Santoro, A., Aubriere, K., Brizzi, G., Collu, M., Corvaglia, P., and Lagasco, F. (2020).On the arrangement of two experimental activities on a novel multi-purpose oating structure concept, pages 291{302.

Sedgwick, H. J. . J. Orecca european o shore renewableenergy roadmap. Electronically.

Versteeg, H. and Malalasekera, W. (2016). An introduction to computational uid dynamics : the nite volume method / h. k. versteeg and w. malalasekera. SERBIULA (sistema Librum 2.0).

West, B. J., Brueckner, K. A., Janda, R. S., Milder, D. M., and Milton, R. L. (1987). A new numerical method for surface hydrodynamics.Journal of Geophysical Research92(C11):11,803{11,824.

Zanuttigh, B., Angelelli, E., Bellotti, G., Romano, A., Krontira, Y., Troianos, D., Su redini, R., Franceschi, G., Cantu, M., Airoldi, L., Zagonari, F., Taramelli, A., Filipponi, F., Jimenez, C., Evriviadou, M., and Broszeit, S. (2015). Boosting blue growth in a mild sea: Analysis of the synergies produced by a multipurpose o shore installation in the northern adriatic, italy. Sustainability, 2015:6804{6853.